Computer Science Review 37 (2020) 100272

Contents lists available at ScienceDirect

Computer Science Review

journal homepage: www.elsevier.com/locate/cosrev

Review Article

Indoor environment propagation review

H. Obeidat [a,*], A. Alabdullah [b], E. Elkhazmi [c], W. Suhaib [d], O. Obeidat [e], M. Alkhambashi [f], M. Mosleh [g], N. Ali [h], Y. Dama [i], Z. Abidin [j], R. Abd-Alhameed [b], P. Excell [k]

[a] Faculty of Engineering, Jerash University, Jordan
[b] Faculty of Engineering and Informatics, University of Bradford, Bradford, UK
[c] Engineering and Information Technology Research Centre, Bani Walid, Libya
[d] Faculty of Engineering, Omar Al-Mukhtar University, Libya
[e] College of Engineering, Wayne State University, Detroit, USA
[f] Women College, Oman
[g] Middle Technical University, Baghdad, Iraq
[h] Khalifa University, United Arab Emirates
[i] An Najah University, Palestine
[j] Universiti Tun Hussein Onn, Malaysia
[k] Wrexham Glyndwr University, Wrexham, UK

ARTICLE INFO

Article history:
Received 4 January 2020
Received in revised form 28 April 2020
Accepted 25 May 2020
Available online xxxx

Keywords:
Constitutive electrical parameter
Dominant direct path
Indoor propagation models
Propagation through Building models
MIMO
Radiofrequency propagation
Ray tracing

ABSTRACT

A survey of indoor propagation characteristics is presented, including different models for path loss, shadowing and fast fading mechanisms, different channel parameters including signal strength, power delay, coherence bandwidth, Doppler spread and angle of arrival. The concepts of MIMO channels are also covered. The study also explores many types of deterministic channel modelling, such as Finite Difference Time Domain, Finite Integration Method, Ray tracing and the Dominant path model. Electromagnetic properties of building materials, including frequency dependence, are also investigated and several models for propagation through buildings are reviewed.

Contents

* Corresponding author.
E-mail address: h.obeidat@jpu.edu.jo (H. Obeidat).

https://doi.org/10.1016/j.cosrev.2020.100272
1574-0137/

1. Introduction

Wireless communication engineers struggle with the dynamic behaviour of wireless radio channels. Wireless channels are more susceptible than cabled channels to noise, interference and similar hindrances [1]. Therefore, they try to establish values of the received signal strength at any location. When a signal arrives at a receiver, the signal strength level follows three scales of variations: the largest scale is range dependent, the signal strength level decaying exponentially; at the second scale the signal strength varies around its mean according to a log-normal distribution. These two scales of variations are found over ranges of the order of 10 to 30 wavelengths, The smallest scale follows a Rayleigh or Ricean distribution, where variations are of the order of 0.5λ [2].

Current market demands require the mobile user to have adequate service coverage anywhere and at any time. Since most people spend most of their time within buildings, having good indoor coverage becomes indispensable. In addition to communication services, wireless infrastructure can be utilized to provide localization. The wireless channel is, in general, varying with time, frequency, space, antenna polarization and environment. Although waves behave similarly in indoor and outdoor environments, the indoor environment has distinctive characteristics.

The aim of this paper is to introduce a survey on indoor radio propagation: understanding this is important for many applications, including location-based services (LBS) [3,4], wireless communications like Personal Communications Services PCS [5] and Wireless Private Branch Exchange WPBXs [6], Wireless Local Area Network WLAN coverage planning [7,8] and Smart Home Systems [9–11].

With the vast expansion of mobile technologies, many indoor applications have become supported by 4G services [6,12] and 5G services [13]. In 5G systems, indoor cells are linked to outdoor base stations through indoor base stations working at millimetre waves [14]. The usage of high data rate Multiple Input Multiple Output (MIMO) systems makes the prediction and planning for indoor systems extremely difficult [6].

The organization of this paper is as follows: Section 2 covers a comparison between indoor and outdoor propagation; in Section 3 the frequency bands allocated for indoor applications are presented; modelling the indoor channel is discussed in Section 4 and two types of modelling, stochastic and deterministic models, are introduced. Section 5 explores the electrical properties with frequency of typical building materials. In Section 6 outdoor to indoor propagation models are presented, and finally, conclusions are drawn in Section 7. Fig. 1 graphically illustrates the organization of the paper.

2. Indoor and outdoor propagation comparison

Similar to the outdoor environment, the indoor environment is also a dynamic environment [15]: diffraction becomes an important phenomenon especially in the absence of Line of Sight (LOS) paths, and scattering from objects of a size comparable to the wavelength also has major effects on signal level [16]. The indoor coverage is further constrained by high wall/floor attenuation and low transmitted power, which result in lower delay spread: typical delay spreads indoors are in the range of tens of nanoseconds while being in the range of tens of microseconds for outdoor environments [16]. This gives the indoor environment the advantage of having higher data rates for communications [1]. In outdoor environments, built-up areas, as well as traffic and people movements, may cause non-negligible variations of the propagation channel in both point-to-point and multicast wireless services, in indoor environments movements of people cause the indoor channel to be time-variant even if both transmitter and receiver are stationary [6]. Note however that Doppler effects are neglected since the velocity within buildings is limited [16]. In the indoor case, a simple nth power law is less likely to be applied for path loss prediction due to its complexity [17].

Indoor propagation analysis depends on a building's geometry where frequency reuse in the building is widely used; however, the interference between the floors makes the propagation analysis more challenging. Ray-tracing techniques are widely used to model the channel in indoor and outdoor environments; however, once the size of any obstacle is comparable to the wavelength, ray tracing becomes invalid: this is the case in many indoor scenarios and as a result, this will place restrictions on frequency bands predicted via ray tracing for indoor environments [18]. Path loss attenuation at the specific frequency allocated for a service can be different in indoor and outdoor environments: for example, frequency-dependent attenuation due to oxygen and water vapour particles will restrict the use of 60 GHz in outdoor environments [19] while it is favourable within indoor environments [20]. Indoor propagation is not affected by winds, storms and rainfall which can affect outdoor received signal strength [21], also path loss dependency on operating frequency tends to be larger in the case of the indoor environment [22].

Propagation power consumption is an unavoidable issue, however in both outdoor and indoor scenarios uplink power should be optimized to maximize battery life, while for the downlink path, in the outdoor case the source power is chosen to give high SNR and low interference with other base stations; however, in the indoor case, WLAN routers are often mounted close to people and therefore the radiated power should be set to minimum to reduce interference and putative health risks [16,23]. Note that indoor channels are very sensitive to the location of the antenna: in a dense environment the wireless propagation channel observed from an antenna mounted at ceiling level may be different from that observed when the antenna is mounted on a desk [24].

3. Frequency allocation

The International Telecommunications Union (ITU) defines the radio frequency spectrum bands, wherein many countries, frequency allocation channels and power levels of Effective Isotropic Radiated Power (EIRP) are different. Other bodies set up the frequency allocation include European Postal and Telecommunications Administration CEPT and Intel-American Telecommunication Commission [25]. Frequency allocation Many organizations run their own local private wireless telephone network called a private branch exchange (PBX): these networks use the 800–2000 MHz range [26]. Within indoor environments, received signal strength becomes weakened due to wall penetration losses, therefore indoor small cells (femtocells) are created to provide coverage without the need to incur additional deployment cost; therefore, Long Term Evolution LTE has used 2500 MHz-2690 MHz spectrum to provide coverage in indoor cells [27]. LTE-A and 5G indoor–outdoor environments are using 3.5 GHz band [28].

Other frequency ranges include Bluetooth at 2450 MHz, IEEE 802.11 [a, b, n, g, ac, ad] in the frequency range 2450 MHz

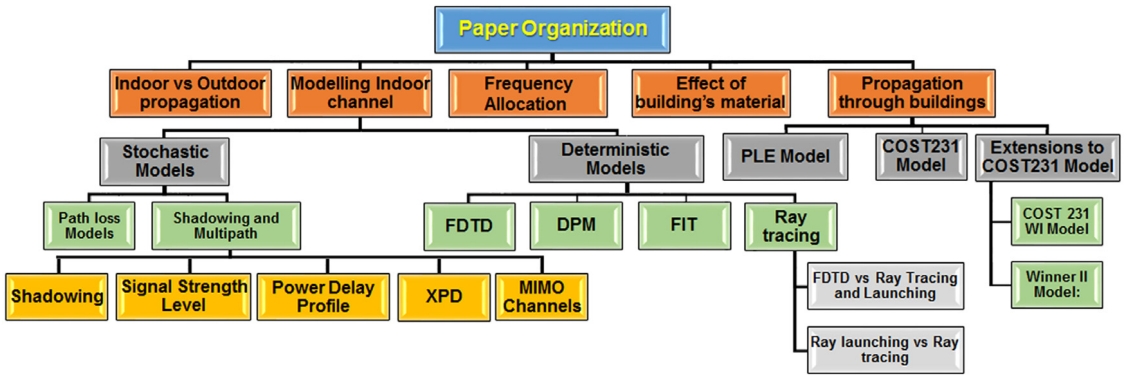

Fig. 1. Detailed structure of the paper organization.

and 5200–5800 MHz bands and free licences 433.05–434.79 MHz, 900–928 MHz, 2400–2483 MHz, 5700–5900 MHz [26] and 60 GHz [29]. The availability for bandwidth is limited as many applications utilize these bands (e.g. at 2.4–2.5 GHz wireless devices are affected by the radiation from microwave oven emissions), hence proper coverage and interference reduction are major considerations [30]. Higher data rates can be achieved by using the bands 17-18 GHz [31], 6.8–8.5 GHz, 24 GHz [32], 28 GHz [33] and millimetre wave bands in the 38 GHz [34], 32.5 GHz, 42 GHz and 58-65 GHz [31], and 73 GHz band [35,36]. In multi-floors environments, channels can be reused on different floors, where non-overlapping channels can be co-located [25].

4. Modelling indoor channels

Generally, there are two main approaches to indoor channel propagation modelling: stochastic and deterministic [37]' although other references also consider semi-stochastic and semi-deterministic models [38]. In stochastic modelling data are collected from measurements, then by using statistical analysis, channel coefficients are characterized to convert the data into parametric equations [38]. The signal level, phases, time of arrival, angle of arrival (AOA) and many signal parameters are characterized by probability distributions to describe their behaviour.

Deterministic modelling depends on laws of physics whereby the electromagnetic wave distributions are solved to estimate the channel parameters at any location in the environment [38]. Environmental details like floor height, doors and windows and their material types and furniture in the environment are carefully considered to predict signal parameters like the signal strength, angle of arrival and time of arrival [39]. The accuracy of the models depends strongly on the detail in which the environmental features are considered [37]. It can be summarized that the stochastic method gives the probability behaviour for an environment parameter at the desired location while the deterministic model potentially gives the exact value. Stochastic models are applied to environments that have similar characteristics to the environment used to construct the model, while deterministic models are created for a specific environment [37].

4.1. Stochastic models (site general models)

Before proceeding with the discussion of this section, it is appropriate to note that, although many models are based on measurements in typical indoor environments like houses and offices, the structure and ingredients are quite different from one culture to another; for instance, houses may be made of brick, concrete, mud, wood, etc. They may also be made of wood and plaster for interior partitions and concrete and brick for exterior partitions, etc. The same applies to "office environment", where some offices are large, and others are small. Some offices have hard partitions which are constructed with the building itself, others have soft partitions made from plaster or wood which are not extended to the ceiling and maybe movable. These generalizations may lead to contradictions with observations in the literature unless the material and details of the environment are specified in detail [40–42].

4.1.1. Path loss models

In this section different path loss models are presented: these include the effects of walls, floors and other complexities of the environment. The mean local path loss at distance d is estimated using the complex frequency response H [43]:

$$PL(d) = \frac{1}{MN}\sum_{i=1}^{N}\sum_{j=1}^{M}\left|H\left(f_i, t_j; d\right)\right|^2 \quad (1)$$

where M and N are the numbers of frequency-response snapshots overtime at distance d and the number of observed frequencies.

i. Local mean estimation

When performing averaging three parameters are considered the window size ($2L$); the number of samples (N) and the distance between the samples (d). [44] performed averaging over the band 1.8 to 5.2 GHz. $2L$ was found to be in the range (5λ-15λ).

Estimating local mean signal is very important to reduce the effect of fast fading. In [45], two procedures were investigated: in the first approach, 120 sample measurements were recorded on circular paths with 0.3 m radius, then averaging was performed; the distance between circles was 0.6 m.

In the second approach, averaging was performed on measurements collected from samples distributed on a 10λ linear path with λ/4 spacing between samples.

In [46] local means were estimated over regions of dimensions $(2\lambda)^2$ dimensions. While in [47] region dimensions was $(3\lambda)^2$, and in [48] and [49] regions were of $(3\lambda)^3$ size.

In [50] $2L$ was set to be 10λ while d was set to 0.38λ. In [51], authors generalized Lee model for the indoor environment over the UHF band. They recommended $2L$ to be 5λ- 10λ.

In [52] analysis was reported that aimed to find the best $2L$ and d; it was found that the best window size was within the range 20λ-40λ with a 1.11λ spacing between samples to ensure that samples were uncorrelated. In [53], authors generalized the work done by [52] over the medium-frequency band, they found that best window size was 2λ; the optimum distance between samples was 0.17λ and the best number of samples was 8.

For Nakagami propagation channels with a small number of multipath $2 \leq m < 4$ (m is the fading parameter), authors in [54] suggested $2L$ be 20λ with 40 samples. While for multipath channels in the range $4 \leq m \leq 8$ it was recommended to set $2L$ to

be 10λ with 20 sample points. In [55] estimating local average signal was conducted in a multi-floor building in the 0.9 GHz-1.9 GHz frequency range; the environment was gridded into $(k\lambda \times k\lambda)$ grids, where k ranged from 6.5–7 for 0.9 GHz and 5–12.5 for 1.9 GHz, comparing to [52], it was found that no approach outperformed the other.

In [56] authors conducted simulations on estimating E field over 3 GHz and 5 GHz, It is found that averaging over an 3D arrangement size a cube with a length of 3.3λ shows an agreement between the local mean magnitude of the Finite Difference Time Domain method (FDTD) and theoretical E-field. Measurements and simulation were conducted over 3 GHz, it was found that as averaging stencil increased the error of estimating E field decreased.

ii. One slope model (OSM)

This is a fast and simple model, also termed as the simplified path loss model. In this model the received power is given by [57]:

$$P_r\,(dB) = P_0\,(dB) - 10n\log_{10}(d) \tag{2}$$

where P_0 is the received power at one metre from the transmitter which can be estimated using a free space formula or experimentally [1], n is the path loss exponent which is calculated using interpolation [58] and d is the distance between transmitter and receiver. Path loss is dependent on range and path loss exponent as shown in Table 1, where OLOS stands for obstructed LOS. In [59] various values of decay index n are presented, the values ranging from 1.2, due to waveguiding effects in corridors, to 6.1 for a dense office environment. In outdoor to indoor propagation at 1.7 GHz [60], decay index n found to be 1.495 for the corridor on a single floor; 1.524 through separated corridors in that building and 3.25 for separate rooms on a single floor and 3.31 in rooms dispersed through a building.

In [42] authors conducted experiments to estimate PLE in different types of buildings at 914 MHz, for grocery stores n found to be less than 2, in retail department stores n found to be slightly more than 2. The effect of using a directional and omnidirectional antenna in UWB systems is presented by [61], the PLE for Omni/Omni, Omni/dir and dir/dir are 1.55, 1.65 and 1.72 respectively.

In [64] it was found that PLE for UWB systems tends to have close results to narrowband systems in LOS scenarios, while for NLOS they tend to be smaller.

Authors in [41] formulated the path loss exponent in mathematical equations as a function of the corresponding excess delay τ_{ex} and whether the propagation is LOS or NLOS:

$$n_{LOS} = \begin{cases} 2.5 + \dfrac{\tau_{ex}}{39} & \tau_{ex} < 15\ ns \\ 3 + \dfrac{\tau_{ex} - 15.6}{380} & 15\ ns < \tau_{ex} < 250\ ns \\ 3.6 & 250\ ns < \tau_{ex} < 500\ ns \end{cases} \tag{3}$$

$$n_{NLOS} = \begin{cases} 3.65 + \dfrac{\tau_{ex}}{536} & \tau_{ex} < 310\ ns \\ 4.2 & 3310\ ns < \tau_{ex} < 500\ ns \end{cases} \tag{4}$$

iii. Linear Attenuation Model (LAM)

The authors in [67] proposed another approach: experiments were carried out over a range of frequencies (0.85, 1.9, 4.0 and 5.8 GHz) and it was concluded that total loss is the sum of free space loss L_{FS} and loss factor in the range of ($\alpha = 0.3-0.6$ dB/m), depending on frequency and building.

$$L\,(dB) = L_{FS}\,(dB) + \alpha d \tag{5}$$

where d represents distance in metres. Eq. (5) can be modified by adding wall losses to overall losses [68].

iv. Dual Slope Model (DSM)

Table 1
Typical path loss exponent for the indoor environment [24].

Building	Frequency (MHz)	n	Reference
Grocery store	914	1.8	[42]
Retail store	914	2.18	[42]
Same floor	914	2.76	[42]
Through floor	914	3.18	[42]
Same floor	1800	4.5	[62]
Through floor	1800	5.3	[62]
Office	900	2.4	[24]
	1900	2.6	[24]
Office/NLOS	2400	3.3	[63]
	4750	3.8	[63]
	11 500	4.5	[63]
Narrow corridor	1500	1.27	[64]
NLOS	1500	3.29	[64]
LOS	1500	1.60	[64]
LOS	2800	1.1	[65]
LOS	7300	1.3	[65]
LOS	4000–6000	1.7	[66]
NLOS	2800	2.7	[65]
NLOS	7300	3.2	[65]
NLOS	4000–6000	3.5	[66]
Factory LOS	1300	1.6–2.1	[24]
OLOS		3.3	[24]
House	900	3.0	[24]

Other models include the effect of diffraction as a potential phenomenon [69]. For this, propagation within an indoor environment was categorized depending on the first Fresnel zone clearance: the "near transmitter propagation" where there is no obstruction in the first Fresnel zone and the path loss exponent is less than 2 due to waveguiding, and secondly "breakpoint propagation" when furniture falls in the first Fresnel zone and path loss exponent becomes larger than 2, as shown in Eq. (6) [70].

$$P_r = P_0 - 10 \times \begin{cases} n_1 \log_{10}(d) & d < d_{bp} \\ n_1 \log_{10}(d_{bp}) + n_2 \log_{10}\left(\dfrac{d}{d_{bp}}\right) & d > d_{bp} \end{cases} \tag{6}$$

where n_1, n_2 are the path loss exponents and d_{bp} is the breakpoint distance. Calculation of the breakpoint distance is done either theoretically as in [70] or experimentally as in [71].

The authors in [69] claimed better performance for the dual-slope model compared to the simplified path loss model since the former has an overall standard deviation of 4.9 dB while the latter has 17.2 dB.

In indoor environments the direct path may not be the dominant path as other rays which are not direct may have a stronger signal, in [72] the one slope model and dual slope models were enhanced by infusing the concept of the dominant direct path in the model instead of using the direct path, authors claimed better performance compared to the original models.

v. Partitioned Model (PM)

In this model path loss is estimated based on predetermined values of n and distance (in metres) between transmitter and receiver [73]

$$L = L(d_0) + \begin{cases} 20\log_{10} d, & 1 < d \le 10 \\ 20 + 30\log_{10}\dfrac{d}{10}, & 10 < d \le 20 \\ 29 + 60\log_{10}\dfrac{d}{20}, & 20 < d \le 40 \\ 47 + 120\log_{10}\dfrac{d}{40}, & d > 40 \end{cases} \tag{7}$$

Measurements show that one-slope and dual-slope models outperform the partitioned model performance [70], Ericsson

Table 2
Indoor power loss exponent [74].

Frequency	Residential	Office	Commercial	Factory	Corridor
900 MHz	–	3.3	2	–	–
1.25 GHz	–	3.2	2.2	–	–
1.9 GHz	2.8	3	2.2	–	–
2.1 GHz	–	2.55	2	2.1	1.7
2.4 GHz	2.8	3	–	–	–
3.2 GHz	–	2.7	–	–	–
2.625 GHz	–	4.4	–	3.3	–
4 GHz	–	2.8	2.2	–	–
5.2 GHz	3, 2.8	3.1	–	–	–
5.8 GHz	–	2.4	–	–	–
28 GHz	–	–	2.76	–	–
60 GHz[(1)]	–	2.2	1.7	–	1.6
70 GHz[(1)]	–	2.2	–	–	–

Table 3
Floor penetration loss factor L_f (m) for m floors [74].

Frequency (GHz)	Residential	Office	Commercial
0.900	–	9 (1 floor) 19 (2 floors) 24 (3 floors)	–
1.8–2	$4m$	$15 + 4(m-1)$	$6 + 3(m-1)$
2.4	10,5	14	–
3.5	–	18 (1 floor) 26 (2 floors)	–
5.2	13[a] (Apartment) (house) 7[b]	16 (1 floor)	–
5.8	–	22 (1 floor) 28 (2 floors)	–

[a]Per concrete wall.
[b]Wooden house.

Table 4
Floor attenuation factor for different buildings.

building		FAF (dB)	
		915 MHz	1900 MHz
Office Building 1 [24].	Floor 1	12.9	–
	Floor 2	5.8	–
	Floor 3	5.7	–
	Floor 4	2.6	–
Office building 2 [24].	Floor 1	16.2	–
	Floor 2	11.3	–
	Floor 3	4.1	–
Office building (San Francisco Pacific Bell) [83]	Floor 1	13.2	26.2
	Floor 2	4.9	7.2
	Floor 3	5.9	1.8
	Floor 4	3.0	3.2
	Floor 5	0.1	8

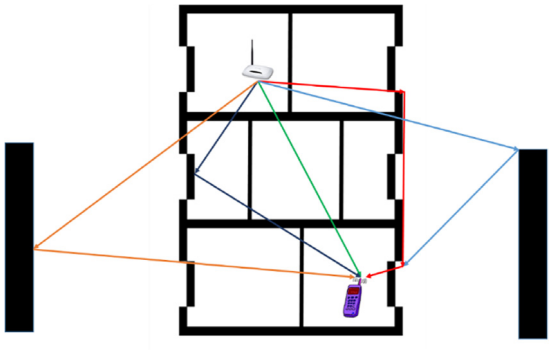

Fig. 2. Propagation through floors.

Radio Systems have taken a similar approach while the path loss has upper and lower limits depending on the fading severity: the path loss exponent was found to be in the range from 2 to 12 as distance increased [17].

vi. ITU-R P.1238 Indoor model

This is a stochastic model that accounts for the losses due to penetration through floors within the same building [74]:

$$L\,(dB) = 20\log_{10} f_{MHz} + 10n\log_{10}\frac{d}{d_0} + L_f\,(m) - 28 \tag{8}$$

where L_f (m) is the floor penetration loss factor which varies with frequency, type of floor and number of floors (m). Based on a large number of measurements, the model gives typical values for both n and L_f (m) for different indoor environments in Tables 2 and 3 respectively. Some guidelines that should be considered when using these tables are given in the source literature [74].

Floor attenuation factor may be superimposed with the path loss exponent; hence, values of n become larger than those in Table 2 [24].

vii. Motley and Keenan Model (MKM)

The wide range of values of n makes the use of the simplified path loss model (one slope model) inadequate and hence these authors proposed other models to be considered for the effect of walls and floors, including consideration of their types and number. The loss in dB is given by [75,76]:

$$L = L_{FS} + L_C + \sum_{i=1}^{I} N_{wi}L_{wi} + \sum_{j=1}^{J} N_{fj}L_{fj} \tag{9}$$

where $(L_{FS}, L_C, N_w, N_f, L_w, L_f, i, j)$ are the free space loss, constant term (loss at $d_0 = 1m$), number of walls, number of floors, wall loss factor, floor loss factor, type of wall and type of floor respectively. It is noteworthy that L_w and L_f were found to be lower as the number of interleaving walls or floors increased [77,78]. This may be related to the fact that the signal will find other paths to propagate, such as corridors and doors in the same floor or via stairs for multi-floor buildings [79], as shown in Fig. 2. Table 4 illustrates values for floor attenuation factor for different buildings, transmitters were positioned at centrally located areas and perimeter areas within wings of each building, at other locations, the transmitter was located within a partitioned office cubicle. Wall and floor losses tend to depend on thickness, types of materials, angle of incidence and frequency [80]; floor loss factor was observed to increase as the frequency increases [81] and losses at oblique incidence tend to be larger compared to normal incidence [82].

viii. COST231 Indoor Model

A more sophisticated model was given by COST231, which adopts the concept of the Keenan and Motley model. The model assumes a linear increase of loss as the number of walls increases, and a non-linear increase of loss as the number of floors increases, due to the decrease in floor losses as their increases; the model is given in Eq. (10) [82]:

$$L = L_{FS} + L_C + \sum_{i=1}^{I} N_{wi}L_{wi} + L_f n_f^{\left(\frac{(n_f+2)}{(n_f+1)} - b\right)} \tag{10}$$

where L_C is the resultant wall losses obtained by applying multiple linear regression to the measurements, b is an empirical constant, L_{wi} is wall loss and L_f is the floor loss. Two types of walls are defined: a light wall which has thickness <10 cm, such as plasterboard, and heavy walls which have thickness >10 cm, such as brick or concrete [82]. Typical values for light wall loss are

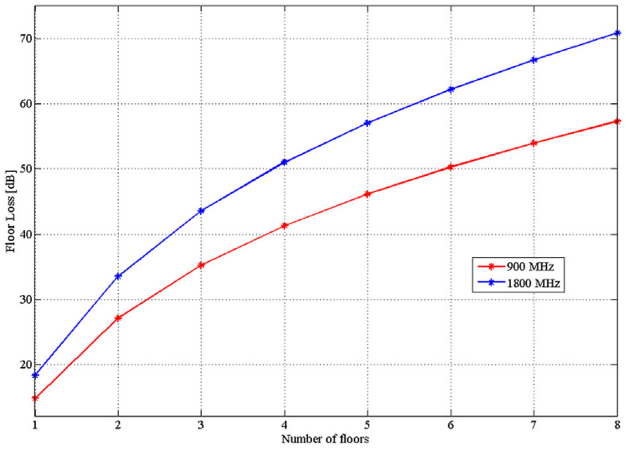

Fig. 3. Floor losses for COST231 indoor model.

1.9 dB at 900 MHz and 3.4 dB at 1800 MHz. For heavy walls, the average loss at 1800 MHz is around 6.9 dB [82]. Typical values for floor losses are 14.8 dB and 18.3 dB for 900 and 1800 MHz respectively. For different types of environments, the empirical constant b found to be 0.46 at 1800 MHz [82].

Fig. 3 shows how individual floor losses decrease as the number of floors increases (in the figure floor losses are aggregated at each floor), but also how floor losses increase as frequency increases.

As mentioned above, the model assumes that wall losses are linear as the number of walls increases, this makes the results to be pessimistic. An extension has been made so that individual wall losses decrease as the number of walls increases: this gives better performance [84].

ix. Average Wall Model (AWM)

AWM was proposed by [8] as a fast design model for indoor radio coverage where few measurements are required as they are collected one metre away from the transmitter and from each wall in the facility. This model is similar to the Motley–Keenan model although the way losses are calculated is different, where losses from the same type of walls are averaged.

The total loss after each wall is the result of multiplication of the average losses by the total number of encountered walls. The first wall loss is estimated at 1 m away from the wall by finding the difference between the path loss estimated from measurements and the losses due to free space propagation, as shown in Eq. (11) [8]:

$$W_1 = P_{r1} - P_0 + 20\log_{10}(d_1) \tag{11}$$

where P_{r1} is the received signal strength after one metre from the first wall, and d_1 is the distance between the point where the P_{r1} measurement was taken and the transmitter. The same procedure is followed for the second wall provided that the loss due to the first wall is excluded:

$$W_2 = P_{r2} - P_0 + 20\log_{10}(d_2) - W_1 \tag{12}$$

where P_{r2} is defined similarly to P_{r1}. In general, the nth wall loss is estimated as shown in the equation below:

$$W_n = P_{rn} - P_0 + 20\log_{10}(d_n) - \sum_{i=1}^{n-1} W_i \tag{13}$$

where P_{rn} is defined similarly to P_{r1} and P_{r2}. To exclude multipath effects, the mean value for all wall loss of the same type is taken as: $(W_{avg} = \frac{\sum_{i=1}^{L} W_i}{L})$. where L is the number of walls of the same type. If a receiver is at distance d from the transmitter, the received signal strength is:

$$P_r = P_0 - 20\log_{10}(d) - \sum_{i=1}^{V} W_i \tag{14}$$

where V is the number of encountered walls between the transmitter and the receiver.

In [85] a comparison study between MKM, OSM, LAM, PM, DSM and AWM over a wide range of frequencies and different antenna polarizations was conducted. The experiments were done using ray-tracing software and were verified by measurements. It was observed that both linear attenuation factor and path loss exponent increased as frequency increased and as polarization was changed from circular to linear. PM shows the worst performance, while DSM gave the best performance and it has a better performance than OSM as it has two path loss exponents; however, the model requires more data in order to give accurate predictions. MKM and AWM show comparable performance while OSM and LAM also have similar behaviour. In the case where the tested environment is a hall or corridor, the study suggests using non-wall dependent models (e.g. DSM, OSM and LAM) to predict the signal strength.

Table 5
Typical values for WINNER II Indoor models [86].

		A	B	X	σ
Indoor office/residential	LOS	18.7	46.8	–	3
	NLOS[a]	36.8	43.8	$5\,(n_w - 1)$	4
	NLOS[b]	36.8	43.8	$12\,(n_w - 1)$	
	NLOS[c]	20	46.4	$5n_w$	6
	NLOS[d]	20	46.4	$12n_w$	8
Indoor or Hotspot	LOS	13.9	64.4	–	3
	NLOS	37.8	36.5	–	4

[a]Corridor-room propagation and light walls.
[b]Corridor-room propagation and heavy walls.
[c]Room-room propagation and light walls.
[d]Room-room propagation and heavy walls.

x. WINNER II project

In the [86] a set of measurements were conducted on different propagation scenarios in the range of frequencies from 2 to 6 GHz. Two general indoor cases were covered, the first being an indoor floor that could be an office or residential, and the second case a very large hall, such as a conference hall or railway station. The path loss is given by Eq. (15) [86].

$$PL = A \cdot \log_{10}(d) + B + C \cdot \log_{10}\left(\frac{f_c}{5}\right) + X \tag{15}$$

where X represents environment-specific term accounts for wall attenuation losses for indoor office NLOS, and $C = 20$ dB for all cases except for room-to-room propagation with heavy walls, for which it is 23 dB. Other parameters are given in Table 5.

n_w is the number of walls and σ is the shadowing fading standard deviation. In the case where transmitter and receiver are on different floors an additional loss is added to the above equation [86]:

$$L_{floor} = 17 + 4\,(n_f - 1) \tag{16}$$

where n_f is the number of floors. The mean values for the Ricean K-factor for the two LOS cases in Table 5 are 7 and 2 respectively. For both cases, the delay spread was found to follow an exponential distribution. The number of clusters in both cases was larger in the NLOS compared to LOS, while the correlation distances are

Table 6
Location variability for indoor office [74].

Frequency (GHz)	$\sigma_L(dB)$	LOS/NLOS
0.8	3.4	LOS
1.8–2	10	
2.2	2.3	LOS
3.5	8	
4.7	2.7	LOS
5.2	12	
5.8	17	
26	2.8	LOS
28	3.4	LOS
	6.6	NLOS
37	2.4	LOS
38	4.6	LOS
	6.8	NLOS
51–57	2.7	
67–73	2.1	

larger in LOS compared to NLOS. Other propagation parameters are discussed in [86].

xi. Path loss and frequency dependence

As the frequency increases, the ability of the wave to bend around corners decreases, causing diffraction to contribute less to overall signal strength and hence path loss tends to be larger at higher frequencies [77,87]. According to [88] it was observed that the path loss exponent does not change with frequency: it was also observed that both path loss and path loss exponent do not change with bandwidth, modulation and polarization of the wave.

In [89] a set of experiments was carried out over the frequency range 3–11 GHz: it was observed that, as frequency increases, the attenuations in NLOS scenarios are more severe compared with LOS cases. Another study on the same frequency range found that path loss exponent, delay spread and power delay profile (PDP) have similar behaviour over this range of frequencies [90]. The frequency dependence of path loss exponent found to be related to LOS existence, as n was recorded to have slightly different frequency-dependence in LOS cases: it was observed to have more dependence on frequency in the NLOS cases [91].

4.1.2. Shadowing and multipath

Hashemi [16] proposed a model for multipath channels. He suggested that the impulse response of the channel is represented by "main waves" including the LOS which may be attenuated. Those waves arrive at the receiver from different scatterers. Each main wave arrives from a different path and encounters different obstacles; the scattered waves arrive with similar delays and attenuations. At the receiver, the resultant wave is the sum of incoming waves and this may have faded due to destructive addition of waves.

Similarly to outdoor propagation, indoor fading occurred on a large scale (path attenuation and shadowing) and on the small scale (multipath and Doppler spread): the channel could also be narrowband or wideband. Probability distributions are used to describe the probability of the signal parameters in the stochastic models.

i. Shadowing and signal strength level

Fading due to shadowing in an indoor environment tends to follow a Log-Normal distribution. Typical values for location variability σ_L for an office are given in Table 6 [74]:

Signal strength levels can be described by many distributions, depending on the circumstances of the experiments. In the case where NLOS is dominant, it was found that signal level follows a Rayleigh distribution [92,93], but in the presence of the LOS component, the signal envelope follows a Rician distribution [94,95]. Experiments in other circumstances show a Log-Normal distribution [96,97], Suzuki distribution [98], Nakagami distribution [99,100], exponential distribution [101] and Weibull distribution [87,100,102].

The Suzuki distribution [103] applies in many locations as it combines the Log-Normal with Rayleigh distributions, so it gives the signal fading due to shadowing, superimposed with the Rayleigh fading due to multipath propagation [98].

The Weibull distribution has the flexibility to cover a range of circumstances, as presented in [104] where measurements are collected in an office environment at 1.1 GHz. Here, different transmitter–receiver separation distances were applied, LOS and NLOS cases and the effect of people motion were considered. Each sample was taken for 60 s to record channel temporal variations. Several different probability distribution functions (PDFs) were tested to fit the measurements: the percentages were as follow: Rayleigh (1%), Lognormal (7.8%) Rician (22.3%), Nakagami (31.8%) and Weibull (37%), Weibull was found to be more evident in LOS propagation. The indoor environment is very complicated, therefore signal parameters will not follow the same behaviour in all environments. Since it has three parameters, the Weibull distribution offers flexibility so that even if the environment changes Weibull still represents the signal level fading [87]:

$$p(x, m, \epsilon, \rho) = \frac{m}{\epsilon}\left(\frac{x-\rho}{\epsilon}\right)^{m-1} e^{-\left(\frac{x-\rho}{\epsilon}\right)m} \tag{17}$$

where (m, ϵ, ρ) are the shape parameter, scale parameter and location parameter respectively. The Weibull distribution becomes a Rayleigh distribution when $m = 2$ and an exponential distribution when $m = 1$ [105].

ii. Power delay profile

The Saleh-Valenzuela (SV) model (along with modifications) is popular and widely used for describing arrival time sequence and amplitude in the case of resolvable multipaths and it was also adopted in the IEEE 802.15.3a and IEEE 802.15.4a models [106]. The model describes the behaviour of multipath in indoor environments, suggesting that rays come in clusters as shown in Fig. 4. The number of clusters tends to decrease with increasing frequency [107] and as the separation between transmitter and receiver is increased [108]. It also tends to follow a modified Poisson distribution [109]; however, in [110] it was stated that it does not follow a specific distribution. Considering the first ray of each cluster and aggregating them together, it was found that the best fit for the amplitude of these rays follows a negative exponential distribution while their inter-arrival times follow a modified Poisson distribution [92]. The amplitude of each individual ray follows a Rayleigh distribution or Normal distribution in the UWB propagation case, while its phase follows a Normal distribution [26]. The number of clusters tends to follow a Poisson distribution [109].

The indoor channel based on the SV model is described by:

$$h(t) = \sum_{l=0}^{\infty}\sum_{k=0}^{\infty} \beta_{kl} e^{j\varphi_{kl}} \delta(t - T_l - \tau_{kl}) \tag{18}$$

where β_{kl} is the multipath gain, φ is the phase associated with the lth cluster and kth ray, l is the number of clusters, k the number of arrival rays within the lth cluster, T_l is the arrival time of the lth cluster and τ_{kl} is the arrival time of kth ray within the lth cluster. Note that the SV model was developed for wideband systems, but it also found to be valid for UWB systems [106].

The work done in [111] was updated by [92] to include the behaviour of the angle of arrival in the indoor environment: they found that the arrival waves tend to be clustered in time and

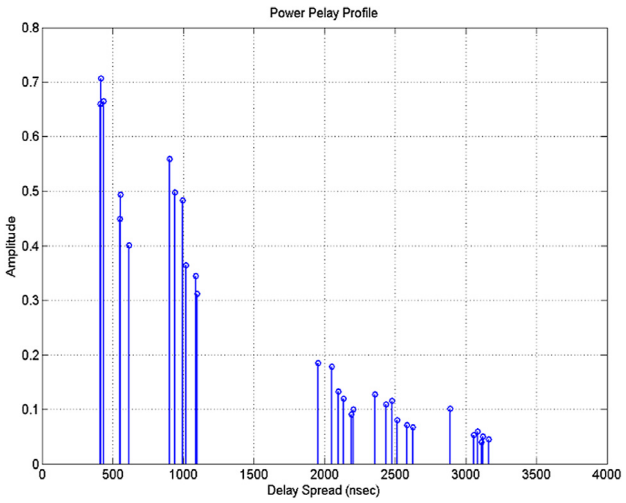

Fig. 4. Saleh Valenzuela model.

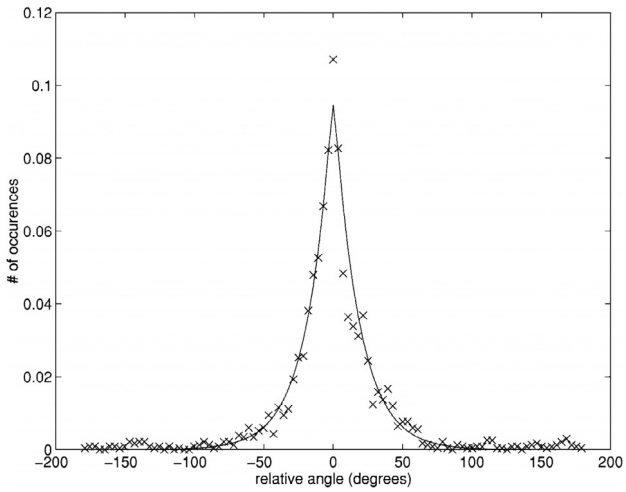

Fig. 5. Histogram of relative ray arrivals with respect to the cluster mean [111].

Table 7
Typical mean value for the angular spread in the indoor environment [74].

	LOS	NLOS
Hall	23.7°	–
Office	14.8°	54°
Home	21.4°	25.5°
Corridor	5°	14.76°

angle as shown in the equation below [111]. For all rays within a cluster the mean of their angles of arrival is known as the *cluster arrival angle* (Θ_i).

$$h(t,\theta) = \sum_{l=0}^{\infty}\sum_{k=0}^{\infty} \beta_{kl} e^{j\varphi_{kl}} \delta(t - T_l - \tau_{kl})\, \delta(\theta - \Theta_l - \omega_{kl}) \tag{19}$$

where ω_{kl} is the arrival angle of the kth ray of the lth cluster. The conditional distribution for Θ_i given that Θ_0 is uniform, where Θ_0 is the first cluster arrival angle, while the kth ray's arrival angle ω_{kl} follows a Laplacian distribution [111].

$$p(\omega_{kl}) = \frac{1}{\sqrt{2}\sigma} e^{-\left|\sqrt{2}\omega_{kl}/\sigma\right|} \tag{20}$$

where σ is the standard deviation. Fig. 5 shows a histogram of relative ray arrival angles: as seen in the figure the best fit is a Laplacian distribution [111]; however, in [112] a set of measurements conducted at 60 GHz found that the best distribution fit was Gaussian while cluster arrival angles tended to follow a Uniform distribution. An extension to current models includes the existence of the LOS path [110] and angle of aperture [113]. Table 7 gives the mean value for the angular spread in an indoor environment.

Delay spread tends to follow a normal distribution and has a clear dependence on the distance between the transmitter and receiver [102]. Typical values for average indoor mean delay spread are in the range of 20–30 ns over the frequency range of 0.9–1.3 GHz [102,114].

In [26] statistics of delay spread σ_{rms} were measured by their mean, median and standard deviation. It was found that LOS propagation has lower metrics compared to NLOS propagation: similar observations obtained by [115] were that σ_{rms} tends to be larger for NLOS cases compared to LOS cases. σ_{rms} was found to be larger as the transmitter–receiver separation increased [43,114] and as the area of the floor became larger [74], however, some studies found that delay spread dependence on the transmitter and receiver separation is insignificant [116]. Eq. (21) shows a

Table 8
Median RMS delay spread in different environments [74].

Frequency	Environment	Median RMS delay spread (ns)
1.9 GHz	House	70
	Office	100
	Commercial	150
2.625 GHz	Office	11
	Corridor	18.53
	Air cabin	11.89
	Factory	69.2
3.7 GHz	House	22
	Office	38
	Commercial	145
5.2 GHz	House	23
	Office	60
	Commercial	190
60 GHz	Office	1.77

proportional relationship between delay spread and floor area (F_a) up to 1000 m^2 at 2 GHz [74]:

$$\log \sigma_{rms} = 0.23 \log(F_a) + 1.1 \tag{21}$$

Paths with longer distances tend to have larger delay spread in propagation between floors [43]. Also, due to more reflection, diffraction and transmission occurring, σ_{rms} tends to be larger, but on the other hand, signal power will decay and may be undetected by the receiver as it may fall below the receiver sensitivity [117]. It was found that increasing the operating frequency caused the mean of σ_{rms} to fall [107,118], while other observations found no relationship between σ_{rms} and the centre frequency [119]. However in NLOS scenarios σ_{rms} was found to be larger as frequency increases [120]. Channel delay spread and path loss exponent are strongly correlated in cases where both transmitter and receiver are directional, with either vertical or horizontal polarization: this can be observed by rotating the receiver as this causes the log of delay spread to vary linearly with its path loss exponent. In cases where an omnidirectional antenna was used, such a correlation does not exist [114,121,122]. Table 8 summarizes the median RMS delay spread in different environments.

The number of detected paths depends on receiver sensitivity and transmitter–receiver separation. Higher sensitivity means that more paths are expected to be detected, however, if the separation is increased the loss of detectable rays will increase. Thus, fewer rays are expected to be received as distance increases [41],

bu [123]. This probability is further reduced in open spaces, compared to a densely built environment, since more reflection and scattering are likely to occur in dense environments: measurements show that the number of detected paths follows a modified Beta distribution [123–125], a Gaussian distribution [97], or a Poisson distribution and, in cases where the threshold is lower, the distribution tends to be Normal [126].

iii. Cross polarization discrimination (XPD)

Signals are transmitted with different polarizations for certain purposes, however, if the signal transmitted passes through an anisotropic medium, then, signal polarization will be affected, causing cross-polar interference and reduction in signal power [17]. For example, if the signal transmitted is vertically polarized, due to reflection and diffraction there will be a small portion which becomes horizontal: the ratio of the horizontal part to the vertical part is known as cross-polarization discrimination XPD [127]:

$$XPD\,(dB) = 20\log_{10}\frac{E_{co}}{E_{cross}} \tag{22}$$

where E_{co}, E_{cross} are the co-polarized and cross-polarized signal strength respectively.

Cross-polarized systems are used to reduce antenna size as the mutual coupling between elements is reduced [128]; it is also used for frequency reuse through polarization diversity [129]. From Eq. (22) it can be observed that a large value for XPD is related to LOS dominant propagation as the signal is not depolarized [130], while a small value for XPD is related to obstructed LO [131]. In [131] it was also observed that there is no strong relationship between path loss exponent and polarization when both transmitter and receiver are co-polarized. XPD may lead to spectrum wasting but, conversely, in MIMO systems polarization diversity is deployed to reduce this effect and to maximize signal power [132,133]. Measurements show an independent relationship between XPD and both azimuth spread and delay spread [128]. As the level of obstruction increases, the cross-polar component will have a similar level to the co-polar component or even higher, due to the effect of wave depolarizing which tends to increase as the level of obstruction increases [133].

σ_{rms} was found to be lower when using a directional antenna compared to an omnidirectional antenna, it was also observed that circularly polarized (CP) waves have a lower σ_{rms} compared to linearly polarized (LP) waves [130]. This is due to the fact that for a singly reflected CP signal where the angle of incidence is greater than the Brewster angle it will be orthogonal to the LOS component, leading to a reduction in multipath interference, this reduction will depress σ_{rms} as the number of rays is reduced [74]. Comparing with the LP case, CP shows a reduction in σ_{rms} by at least 20% in Obstructed LOS scenarios [131], In order to clarify the source of a reduction in σ_{rms}, the authors in [131] measured the σ_{rms} for omnidirectional LP, directional LP and directional CP antennas. In their results, it was concluded that differences in propagation estimated parameters are due to polarization rather than antenna radiation.

In [132] an extensive set of measurements had been undertaken on a 4×4 MIMO system operating on 2.4 GHz with 200 MHz bandwidth: the measurements included five-time snapshots to guarantee reliable observations, three antenna spacings, 1601 frequency segments and four polarizations, VV, HH, VH and HV where V denotes vertical polarization, and H denotes horizontal polarization, the experiments were carried out in three scenarios: in the case of NLOS both HH and VV behaved similarly and the same observation was noted for VH and HV. Similar observations were recorded in [134]: a partition loss model was proposed and it was observed that wall losses tend to be smaller in the case of cross-polarization, while the path loss exponents tend to be larger for co-polarized propagation [132], it was also observed that XPD reduced by half when propagation was changed from LOS to NLOS. Time delay spread tends to be less for co-polarized propagation over shorter distances, while it becomes similar for larger distances. In terms of capacity, with LOS co-polarized offers larger capacity, while for NLOS cross-polarization has a larger capacity and when the spacing between antennas decreases the performance differences between co-polarized and cross-polarized propagations increase: this is also confirmed by [135].

In [128] the XPD of each path was investigated. The study showed that for NLOS the XPD is insensitive for azimuth and delay while it shows a sensitivity for co-elevation. XPD tends to follow a Gaussian distribution for both LOS and NLOS and tends to be time-varying due to its dependency on the propagation channel [135].

iv. MIMO channels

MIMO utilizes diversity techniques to increase data rates: coverage, throughput and capacity are further improved [136]. Channels used to describe Single Input Single Output (SISO) have to be updated for MIMO channels, models for which can be classified into narrowband and wideband, physical and analytical [137]. Many models have been proposed for the indoor MIMO channel: examples include the Extended Saleh-Valenzuela Model, the two ring model [138], IST METRA model, IST SATRON models [136] and WINNER II model [86].

In [139], the relationship between path loss and channel capacity was investigated for an indoor MIMO channel. It was found that for fixed transmitted power the median capacity of the channel tends to decrease linearly with path loss. For a symmetric transmitter and receiver array arrangement median capacity is [139]:

$$C_{median} = 0.17 \cdot N \tag{23}$$

where N is the number of antenna elements. A massive MIMO algorithm for indoor scenarios was proposed in [140], with an algorithm similar to the Kronecker and Weichselberger models [141,142]. The channel matrix is divided into two matrices: the first part, termed as the fixed part, is related to LOS propagation, while the second part is termed the random part and it considers the effects of reflection, scattering and diffraction. The random part is further modelled into eigenvector matrices of the transmitter and receiver and in terms of coupling matrices between the transmitter and receiver sides, which depend on the experimental data. The model showed better fitting compared to the Kronecker and Weichselberger models.

Channel parameters were investigated in [143]. In the NLOS scenario, the received signal strength tends to follow joint Rayleigh and double-Rayleigh distributions; while in LOS it tends to follow a Rayleigh distribution. The angle of arrival and angle of departure were found to have a tendency to follow a Laplacian distribution. The study also found that numbers of clusters tended to follow a log-normal distribution.

4.2. Deterministic models (site specific models)

In a deterministic model, the channel and signal parameters are determined for every location in the environment. The most accurate results would be obtained by solving Maxwell's equations; however, such a task is effectively impossible even with high-speed computers due to the complexity of specifying boundary conditions [144]. Deterministic techniques for indoor propagation include the Ray tracing [144], the FDTD [49], the Dominant Path Model (DPM) [145] and the Finite Integration Technique [146].

4.2.1. Ray tracing

Most deterministic models nowadays adopt the ray-tracing technique for indoor propagation prediction since it requires less computational time compared to FDTD [147]. As long as the wavelength is smaller than the sizes of the obstacles the waves can be considered as rays and ray theory can be applied [148]. Both transmitter and receiver are considered as source points where wave propagation between them is described as rays. Early ray tracing models adopted geometric optics and considered only reflection and refraction [149], but later the effect of diffraction was included enhancing propagation parameter prediction [150]. Rays can be generated by two methods; the first method is performed by launching many rays through many angles where only those which have power above a certain threshold are considered: this method is known as "*Ray launching*". The second method considers only the paths between the transmitter and the receiver, where the ray paths are established by considering multiple images of the transmitter which occur as a result of reflection off walls. The path is found by drawing straight lines between the multiple images to the receiver: this method is known as "*Multiple images*" [151]. This method suffers from the exponential growth of the computational time as the number of reflections increases; however, it has been successfully adopted for semi-deterministic models where the main propagation paths are identified deterministically while other complex propagation parameters are empirically calculated. The ray launching technique is however usually preferred as it deals with diffracted and scattered rays along with the reflected rays.

Due to the absence of LOS in many indoor propagation cases, including the effects of diffraction and scattering become inevitable. The authors in [152] proposed a 3D ray-tracing method based on geometrical optics and the uniform theory of diffraction (GO/UTD) for indoor environments at 1.8 and 2.5 GHz. The simulations were compared to measurements for both narrowband and wideband cases: in the narrowband case the signal mean level along with the statistics of its variations were estimated correctly; in the wideband case both the amplitudes and arrival times of the multipath components were found to follow the predicted behaviour.

The combination of UTD and shooting and bouncing rays (SBR) provides an accurate 3D analysis of indoor propagation [153]. The advantages of fast computation speed possible with SBR and the ray accuracy detection from the multiple images method can be combined to produce a hybrid which enhances signal predictions. The method starts with the SBR to determine the ray paths and multiple images are then applied to adjust the ray trajectory [154]. The received electric field of the ith ray is calculated as [150]:

$$E_i = E_0 U_{ti} U_{ri} L_{FSL}(r) \times \left[\prod_j R_j \prod_p T_p \prod_l D_l A_l \left(S_l, S_l'\right) \right] e^{-jkr} \qquad (24)$$

where $L_{FSL}(r)$, $U_{(t/r)i}$, R_j, T_p, D_l, S_l, S_l', k: are the free space loss, transmitter/receiver radiation pattern, reflection coefficient of the jth reflection, transmission coefficient of the pth transmission, diffraction coefficient of the lth diffraction, the path length from the transmitter to diffraction edge, path length from diffraction edge to the receiver and wave number respectively.

If a trade-off between database complexity and accuracy is necessary, in [155] the authors found that in the case where the model details have errors, the predictions become more sensitive in the case of NLOS; they also found that RMS delay spread is sensitive to the errors in object size more than errors in the object's lateral face, the study also found that, in the case of changing the values of material electrical properties, walls will have more impact on signal predictions compared to floors and ceilings [155].

Ray-tracing techniques can also be accelerated by using space divisions and simplifications into 2D and 2.5D map techniques [154].

Several commercial software tools are available to simulate the environment in a 3D structure and to emulate the wave propagation to predict channel parameters. The accuracy of these predictions depends on how accurately the environment model is constructed. Popular software packages include Wireless InSite® [156], WinProp® [157], EDX SignalPro® [158] and iBWAVE Wi-Fi® [159].

Ray launching vs Ray tracing

Ray tracing suffers from exponential increments of computational time as the number of interactions increases, while ray launching shows linear dependency. On the other hand, ray launching suffers from the disadvantage of constant angle increment, which means that some of the surfaces, such as corners, may not be hit [148]. Also, even if the incremental angle were small, as the receiver is moved further away from the transmitter more pixels will be lost; however, by using a reception sphere, it can capture the rays in the vicinity adequately.

Ray tracing is suitable for point to point prediction while ray launching is suitable for area prediction [148]. One possible way to reduce the computational time is by using intelligent ray tracing (IRT) [160]. Using the basic generic ray tracing (GRT) it was observed that while receiving a large number of rays, most of the energy is delivered by a small number of rays: those rays are almost the same for closed-receivers. It was also observed that the visibility between walls and edges is independent of transmitter location, thus by doing pre-processing for the environment the visibility relationships are stored and used for signal prediction: this method removes the redundancy in pathfinding [160]. On the other hand. by using IRT the prediction time is much less than the GRT, although less accurate results are obtained due to pre-processing [161].

The intelligent ray launching (IRL) method has been proposed as a modification of the ray launching technique [117,162]. The environment under study is divided into a large number of cubes which take into account the specific nature of the environment like walls, floors and roofs. The method considers the LOS cubes with the transmitter, where the direct paths are determined and secondary cubes are considered for reflection and diffraction; the method also considers the phenomena of Intelligent Vertical Diffraction which is responsible for counting the number of rooftop diffractions, and finally the Intelligent Horizontal Reflection and Diffraction which trace the rays until they fall below a certain threshold. The total number of launched rays required at the start in order to speed up the computation time is given by Eq. (25) [117]:

$$N = 2XY + 2(Z-2)(X+Y-2) \qquad (25)$$

where (X, Y and Z) are the number of cubes in the x, y and z directions respectively.

4.2.2. Finite Difference Time Domain (FDTD)

Maxwell's equations provide the solution to estimate the signal parameters everywhere, however finding analytical solutions is not always possible and hence approximations and assumptions have long been adopted as an alternative way to solve Maxwell's equations. One of the well-known methods is by using the FDTD method to build a deterministic model for the indoor environment [49,163]:

The FDTD is a time-domain solution that can cover a wide range of frequencies [164]. The main idea is to replace the Maxwellian derivatives with finite difference approximations

which can be evaluated at each point in space and time [165–167].

The grid size should capture the changes in the electromagnetic field, therefore incremental size in all dimensions (Δx, Δy and Δz) should be much less than one wavelength ($\approx \frac{\lambda}{10}$ to $\frac{\lambda}{20}$). The differential increment of time Δt plays a major role in determining the computational time required. In cases where all spatial steps are equal, a stability criterion is defined in [168], this ensures that the electromagnetic wave will not exceed one lattice in one time step:

$$\Delta t \leq \frac{\sqrt{\varepsilon\mu}}{\sqrt{\frac{1}{(\Delta x)^2}+\frac{1}{(\Delta y)^2}+\frac{1}{(\Delta z)^2}}} = \frac{\Delta x}{\sqrt{d}u} \tag{26}$$

where d is either 1, 2 or 3 and represents the dimension of the FDTD structure; u is the velocity of the wave within the medium. Although it requires very large computation time and memory, FDTD is a more powerful tool compared to other numerical methods such as Finite Element Method FEM [169].

The FDTD method can predict the best deployment of receiver antenna, access points and repeaters within the facility [170]. The method had been applied in an indoor scenario in an area of 990 m^2 at 433 MHz [171]: the results showed a standard deviation of about 15.5 dB but it was observed that the resource requirements tend to increase exponentially with frequency as the dimension of the simulated environment increases.

In [172] a full-wave description for an indoor office at WLAN and WiMAX frequencies were estimated using FDTD. The authors found that the path loss exponent was estimated accurately, while the standard deviation for the estimated path loss level was around 5.5 dB.

Another technique that has been applied is the Multi-Resolution Frequency Domain Parflow (MR FDPF) approach. This follows a similar approach to the FDTD method, but it is conducted in the frequency domain [162]. It consists of two stages: the pre-processing stage which is done once as it depends on the scenario only and the propagation stage which deals with the boundary conditions. Compared to FDTD, it has lower complexity as it solves the Maxwell Equations in the frequency domain and the pre-processing also reduces the computational task size [162].

FDTD vs Ray Tracing and Launching:

The FDTD is a time-domain technique which has the advantage of programme simplicity; however, it suffers from a very large computation time requirement [164]. Ray tracing and launching are frequency-domain techniques and hence narrowband, although they have smaller computation times compared with FDTD [164]; however, the programming is more complicated and also in complex geometries many rays cannot be traced. Using low frequencies in indoor environments, many objects may be smaller than the wavelength and in these circumstances, the UTD will no longer be applicable [173]. For 2D FDTD simulation, the total number of numerical operations is [174]:

$$F_{FDTD} = \sqrt{\varepsilon_r} \cdot N_{FDTD} \cdot (N_{FDTD} + 2N_{PML})^2 \tag{27}$$

where N_{FDTD} is the number of FDTD grids and N_{PML} is the thickness in grid elements of the absorbing boundary of the perfectly matched layer (PML).

The total number of numerical operations for the Ray Launching technique is [174]:

$$F_{RL} = N_{RL}^2 \cdot i\,(i+1) \tag{28}$$

where N_{RL} is the number of discretization steps, and i is the number of iterations. As seen, the complexity orders for the 2D FDTD and Ray launching methods are around $\sim N_{FDTD}^3$ and $\sim N_{RL}^2$ respectively [164].

A hybrid technique combining FDTD and ray launching has been proposed to reduce the computational time and to increase prediction accuracy [175]. The environment is divided into two main categories: the places which have irregularity are studied by the FDTD method, which has better performance in these kinds of regions. Small objects are treated as scatterers, in this case, the FDTD is applied to obtain the scattering coefficients which will be used by the ray-optical techniques [173]. Other regions will be studied by ray launching which has the same performance compared to FDTD but with less computational time. The total number of numerical operations for the proposed hybrid technique T is [175]:

$$T = k_{RL}\left(N_{FDTD}^2 - N_{RL}^2\right) + k_{FDTD}N_{FDTD}^3 \tag{29}$$

where k_{RL} and k_{FDTD} are the complexity factors for ray launching and FDTD respectively. The hybrid technique has been claimed to be useful especially for inhomogeneous walls [176].

A similar hybrid technique is proposed in [177], where many scenarios have been presented: better results are observed by using the hybrid technique. The correlations between the measured and hybrid results were 0.84 and 0.83 for the LOS and NLOS propagation respectively; in terms of averaged standard deviation error, the results were 1.85 for LOS propagation and 3.62 dB for the NLOS propagation. The correlations between the measured and ray tracing results were 0.54 and 0.73 for the LOS and NLOS propagation respectively, while their averaged standard deviations were 3.42 dB and 7.18 dB for the LOS and NLOS propagation respectively.

4.2.3. Dominant path model

Ray propagation inside buildings has been studied using stochastic and deterministic formulae. The COST 231 model is considered as one of the most popular empirical methods, however, this model assumes that the direct ray between the transmitter and the receiver is the dominant path [178], which is not the case in most scenarios and in such cases it will contribute less to the total received power [145].

Ray tracing (deterministic model) on the other hand considers many hundreds of rays travelling between the transmitter and receiver, while only a few rays contribute 95% of the total received power. Considering all of the rays will take a long computational time [179]; even using pre-processing the computation time is relatively high [5,180]. Another limitation in using this approach is the demand for having fine details of the building. Inaccurate modelling of the building will cause the rays to be non-representative of the environment. Ray tracing also suffers from time-variant effects, opening doors and windows, moving furniture and people affect the wave propagation: these time-variant effects cannot be considered in the ray tracing models.

The Dominant path model approach (DPM) is similar to the Motley and Keenan method, however instead of considering the direct ray, the dominant rays are considered instead [181]. It considers the main rays which contribute most of the energy, hence using this model will reduce the requirement of having a fine detailed simulated environment; it also reduces the computational time as it considers fewer rays. As this model considers specific information about the environment it shows a time-invariant behaviour which makes it attractive [181]. Fig. 6 illustrates the main ideas for the Motley–Keenan model, ray-tracing model and DPM.

In DPM two main procedures are applied, determination of dominant paths and prediction of signal strength [181]. In the first procedure, the environment is divided into grids, then the first stage considers the transmitter and surrounding grids: transmission losses are computed and those grids are called pixels. The next step is to consider the neighbouring points for each

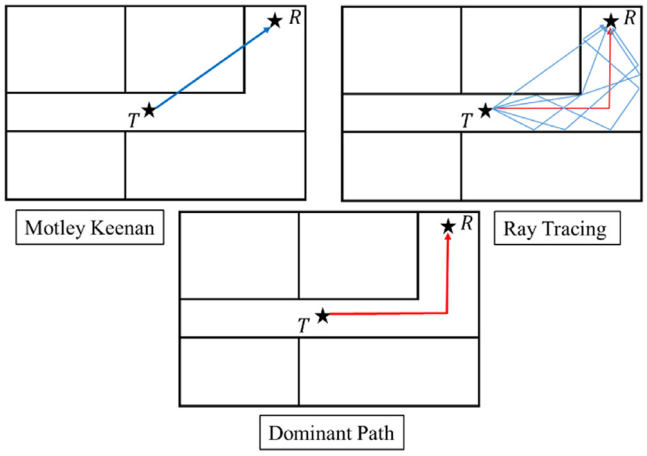

Fig. 6. Motley Keenan model, Ray tracing and DPM.

pixel, and the same procedure is applied, then by linking the pixels with least transmission losses the incoming vectors are identified [182]. Finally, the dominant paths are chosen; depending on how many paths are required the computation time will vary [145]. In the case of a single path, each pixel is reached by a single incoming vector: this will end up with a series of selected pixels starting from the prediction point, then the first neighbour pixel, then the second neighbour pixel and so on until it reaches the transmitter. In DPM the dominant paths are selected depending on many parameters including the number of interactions, the path lengths between the transmitter and the receiver, the number of transmissions and the material properties of obstacles on the path. Most selected paths are those with the shortest distances, or having a smaller number of interactions, or having fewer transmissions [145].

As mentioned above, the number of dominant paths controls the computation time. If the rays pass through the same rooms and walls they can be represented by a single DPM (each dominant path represents different rays); however, if rays pass through different walls and rooms they cannot be represented by a single path [182].

The prediction of signal strength is accomplished using a neural network rather than using UTD since this method does not consider diffraction or reflection points [182]. The input parameters for the neural network include transmission loss, waveguiding effect, free space loss at distance l, and total bent angle [182]. Minimum losses for the DPM are computed as in Eq. (30) [182]:

$$L = w_{FS}L_{FS} + \frac{w_l}{\theta_L}\sum_{i=1}^{p}\theta_i + w_T\sum_{j=1}^{k}T_j - \alpha_{wg} \tag{30}$$

where L_{FS} is the free space loss; w_{FS}, w_l and w_T are weighting factors for free-space loss, interaction loss and transmission loss respectively; θ and θ_L are the change in direction of propagation and normalization factor respectively; t_j is loss due to transmission and α_{wg} is the effect due to waveguiding.

Eq. (30) also includes the effect of waveguiding, which depends on wall material types, their orientation and distance to the propagation path. The effect of waveguiding increases as the wall losses are reduced and as the wave is closer to the wall [145]. A mathematical representation of the waveguiding effect can be found in [182].

Table 9 shows a performance comparison between different models. The table shows the standard deviation for the prediction models compared to measurements [145]. As shown, the DPM shows better performance compared to other prediction models.

Table 9
Performance comparison between signal strength prediction models [145].

	Ray tracing	DPM	Motley–Keenan
Transmitter 1	12.11 dB	5.85 dB	11.39 dB
Transmitter 2	7.23 dB	6.36 dB	9.83 dB
Transmitter 3	9.76 dB	5.64 dB	6.04 dB
Transmitter 4	6.04 dB	5.12 dB	5.82 dB

In [161], IRT was compared to DPM: although both methods share the property of fast processing, in terms of prediction accuracy the former shows less accurate results in the case where the receiver is far away from the transmitter. The authors in [183] extended the algorithm by considering the multi-floor propagation case and the effect of using a directional antenna: the result was a claimed improvement in performance.

4.2.4. Finite Integration Technique (FIT)

In contrast to the FDTD technique, a discretization in time and frequency of Maxwell's Equations in integral form has been developed, namely the Finite Integration Technique (FIT). This technique is valid for a wide range of frequencies ranging from static up to optical frequencies [184]. The principle was first presented by Weiland [185] and can be summarized as converting the open boundary problem into a bounded one; in other words, the target problem is enclosed by a domain called the calculation domain, and this is gridded into a small mesh [186]. The grids are categorized into two orthogonal meshes where the spatial discretizations of Maxwell's Equations are applied: the primary grid has electric voltages e_i on the edges of the grid while it has magnetic flux on each facet b_j; on the secondary grid, the magnetic voltages h_i are on the edges while the electric flux values d_u are on the facets. Faraday's law is applied to the primary grid while the Maxwell–Ampere law is applied to the secondary grid [184].

Applying Faraday's law on the primary edge is equivalent to equating the sum of electric voltages on the edge of a facet to the rate of change in time of the magnetic flux that comes out from the facet [184].

$$\oint \vec{E}\cdot d\vec{s} = \frac{-\partial}{\partial t}\iint \vec{B}\cdot d\vec{A} \tag{31}$$

$$\sum_{facet} e = \frac{-\partial}{\partial t}b_n \tag{32}$$

Applying Equation (32) to all sets of grids can be represented in a matrix form [184] thus:

$$\begin{bmatrix}1 & 1 & -1 & -1\end{bmatrix} \times \begin{bmatrix}e_i\\ e_j\\ e_k\\ e_l\end{bmatrix} = \frac{-d}{\partial t}[b_n] \tag{33}$$

The above equation may be represented as [187]:

$$\boldsymbol{C}\cdot\boldsymbol{e} = \frac{-\partial}{\partial t}\boldsymbol{b} \tag{34}$$

Possible values of $\boldsymbol{C}$ are (−1, 0, 1). Gauss' law of magnetism is updated in the same manner: the sum of all magnetic flux from one grid should equal zero, so for all grids, the equation becomes [187]:

$$\boldsymbol{S}\cdot\boldsymbol{b} = 0 \tag{35}$$

where $\boldsymbol{S}$ is called the divergence matrix. Similar procedures are adopted for the secondary set of meshes: the Ampere law (as

improved by Maxwell) and Gauss law of electricity are given by [187]:

$$\tilde{\boldsymbol{C}} \cdot \boldsymbol{h} = \frac{-\partial}{\partial t}\boldsymbol{d} + \boldsymbol{j} \tag{36}$$

$$\tilde{\boldsymbol{S}} \cdot \boldsymbol{d} = \boldsymbol{q} \tag{37}$$

where $\tilde{\boldsymbol{C}}$ is the dual discrete curl matrix and $\tilde{\boldsymbol{S}}$ is the dual divergence matrix, $\boldsymbol{h}$ and $\boldsymbol{d}$ are constructed similarly to $\boldsymbol{e}$ and $\boldsymbol{b}$.

Material coefficients are further calculated to reduce instability occurring due to spatial discretization. The material coefficients link the two sets of orthogonal grids: these coefficients depend on the averaged material parameters and the grid's resolution [184].

The technique can be combined with advanced numerical methods to achieve optimum modelling for curved simulated structures, however, the computational time is extremely large when using a state-of-the-art code, such as Computer Simulation Technology (CST) Studio Suite®, which is commercial software based on FIT [186].

In [188], a study comparing ray tracing and FIT was conducted on an area of 400 m^2. Different frequencies with different spatial detailing were investigated and it was observed that as the spatial detailing increased and as the frequency adopted decreased the error standard deviation for FIT was found to be in the range of 1.1–2.4 dB, while for ray tracing it was found to be in the range 0.8–4.6 dB. Ray tracing showed better results at 400 MHz, while at 900 MHz the FIT showed more accurate results. Both methods showed a comparable and accurate estimation of the delay profile envelope [188]. According to [146] FDTD and FIT may replace ray tracing in the future as computer capabilities increase.

Other numerical methods have also been applied to solve Maxwell's Equations, including a hybrid parabolic equation-integral equation method (PE-IEM) [189] which obtained good estimation with much less time and memory requirement compared to FDTD. Also, the Method of Moments (MoM) [190] was used in a hybrid technique combining the 3D ray launching method and the MoM [171]. The 3D ray launching method was preferred due to its fast computation time, however, the algorithm lost much accuracy when the obstacle sizes were comparable with the wavelength and therefore MoM was used in those regions to get more accurate results [191].

5. Effects of building materials

Fresnel coefficients are required to solve the reflected, transmitted and diffracted rays; however, those parameters are functions of complex permittivity, therefore the type of material used in constructing the building has a significant effect on the wireless channel in the indoor environment. Material dependency on operating frequency plays a major role in determining radio coverage: as shown in Eq. (38) the attenuation rate A (dB/m) is a function of conductivity σ and relative permittivity ε_r [192].

$$A = \begin{cases} 1636\dfrac{\sigma}{\sqrt{\varepsilon_r}} & \text{Dielectric} \\ 545.8\sqrt{\sigma f_{GHz}} & \text{Conductor} \end{cases} \tag{38}$$

Complex permittivity is a function of ϵ_r, σ and frequency [193]:

$$\epsilon_c = \epsilon_0\epsilon_r - j\frac{\sigma}{\omega} \tag{39}$$

Both ϵ_r and σ are frequency-dependent as shown in Eqs. (40) and (41) respectively:

$$\sigma = \alpha f^{\beta} \tag{40}$$

Table 10
Material frequency-dependent parameters [192].

Material	(ρ)	(α)	(β)	Frequency (GHz)
Vacuum	1	0	0	0.001–100
Concrete	5.31	0.03265	0.809	1–100
Brick	3.75	0.038	0	1–10
Plasterboard	2.94	0.0116	0.7076	1–100
Wood	1.99	0.0047	1.0718	0.001–100
Glass	6.27	0.0043	1.1925	0.1–100
Ceiling board	1.5	0.0005	1.1634	1–100
Chipboard	2.58	0.0217	0.78	1–100
Floorboard	3.66	0.0044	1.3515	50–100
Metal	1	10^7	0	1–100
Very dry ground	3	0.0015	2.52	1–10
Medium dry ground	15	0.035	1.63	1–10

$$\epsilon_r = \rho f^{\gamma} \tag{41}$$

where f in GHz, typical values of (α, β, ρ) for different types of materials are given in Table 10, while $\gamma = -0.1$ or -0.4 for medium dry and wet grounds respectively, but zero elsewhere [192].

A comprehensive review of material properties and their relationship with frequency was presented in [194]: the values given there are repeated in Table 11 and are for specific frequencies and measurement conditions [194]:

In [195], a set of measurements was carried out on different material samples over the range 2.32–2.48 GHz using vertical and horizontal polarization. The investigated materials included concrete, wood, glass, chipwood and thick wood, the results showed no clear loss dependence on operating frequency within the examined range, it also showed that penetration losses tend to increase when switching from horizontal to vertical polarization, except for the concrete samples.

A set of measurements was conducted to explore the relationship between the dielectric constant of building materials and frequency [196]. The investigated materials included wallboard, cloth office partition, structural wood, wooden door, plywood, glass, Styrofoam, bricks and concrete blocks. Detailed dimensions and specifications for the materials are presented in [196]. The wallboard was tested over the range 0.62–13.92 GHz: its ε_r has almost no dependence on frequency, this was also observed for structural wood which was tested over the range 0.81–14.11 GHz, Styrofoam over the range 0.52–13.82 GHz and for concrete blocks over the range 2.02–6.82 GHz. Cloth partition walls were examined over the range 0.52–13.82 GHz and it was found that ε_r tended to decrease slightly with frequency within the range 1.36–1.07; a similar behaviour was recorded for a wooden door which was examined over the range 1.01–14.31 GHz and plywood over the range 2–14.6 GHz, where their corresponding ε_r were in the ranges 2.08–1.98 and 2.55–2.35 respectively. On the other hand, some materials tend to have larger ε_r as frequency increases, as in the case of glass and bricks: glass was tested over 1.01–14.31 GHz while bricks were tested over 1.01–7.01 GHz. Their corresponding ε_r were 6.35–6.71 and 3.73–4.48 respectively. Fig. 7 summarizes the dielectric relationship with frequency for measurements recorded in [196].

In [197], the authors aimed to measure the reflection coefficient for different material types over the X band (8–12.5 GHz). The investigated materials included Polyvinyl chloride (PVC), Beechwood, Sipo, plaster, plaster with silica, mortar and concrete with different water to cement ratios. The materials were assumed to be homogeneous, dry and at room temperature. Mortar is different from concrete as it is made from small grains of sand where the maximum diameter for the grain is 4 mm, while the maximum diameter for concrete is 16 mm. Table 12 gives the mean values for complex permittivity.

Table 11
A summary of material properties presented in [194].

Material	ε_r	σ	Freq. (GHz)	Thickness (m)	Notes
Brick	4.62	0.0174	1.7	–	–
	3.7–4	0.0200	3	0.015–0.0215	0% water volume
	3.7–4	0.0600	9	0.015–0.0215	0% water volume
	3.7–4	0.8	24	0.015–0.0215	0% water volume
	19	0.2917	3	0.015–0.0215	30% water volume
	14	1.1875	9	0.015–0.0215	30% water volume
	4.11	0.0364	18	–	–
Concrete	7	0.0150	0.9	–	Reinforced Concrete
	7	0.0300	1.8	–	Reinforced Concrete
	2	0.0278	1	–	Aerated
	8	0.0833	3	0.02	w/c 22%
	10	0.0833	3	0.0195	w/c 28%
	7	0.1250	3	0.021	w/c 32.5%
	6	0.1667	3	0.2	w/c 40%
	7	0.2453	9	0.0195	w/c 28%
	6.5	0.2830	9	0.021	w/c 32.5%
	6.5	0.1887	9	0.189	w/c 34%
	6	1.3333	24	0.0195	w/c 28%
	5.5	2.3693	24	0.021	w/c 32.5%
	6.5	1.3333	24	0.189	w/c 34%
	6.2	1.8114	95.9	–	Hardened concrete
Wood	2.15	0.0038	1	0.005–0.03	Oven Dry wood $p_0 = 0.7$ g/cm^3
	1.95	0.0479	10	0.005–0.03	Oven Dry wood $p_0 = 0.7$ g/cm^3
	2.5	0.2867	60	0.005–0.03	Oven Dry wood $p_0 = 0.7$ g/cm^3
	1.9	0.2639	100	0.005–0.03	Oven Dry wood $p_0 = 0.7$ g/cm^3

Table 12
Mean complex permittivity for investigated materials [197].

Material	Complex permittivity
PVC	$4.34 - j0.028$
Beechwood (S)	$3.81 - j2$
Beechwood (P)	$4.54 - j0.23$
Sipo	$3.7 - j0.17$
Plaster	$5.74 - j0.06$
Plaster (80%) and Silica (20%)	$4.33 - j0.095$
Mortar	$7.1 - j0.27$
Concrete (water/cement = 0.5)	$7.7 - j0.33$
Concrete (water/cement = 0.7)	$6.9 - j0.4$

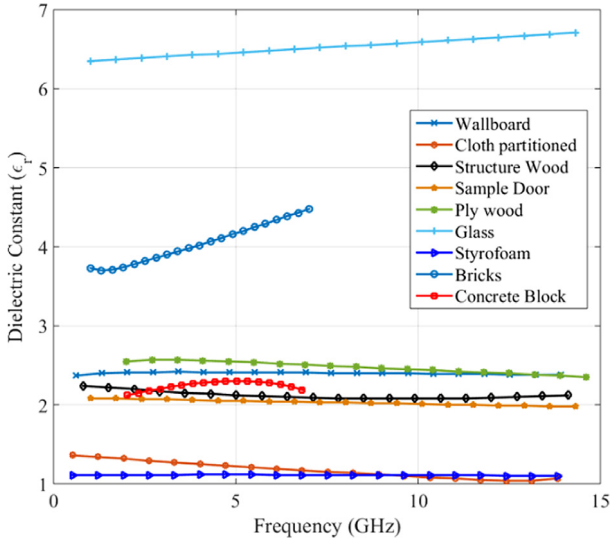

Fig. 7. Variation of dielectric constant with frequency for measurements collected in [196].

Where S and P respectively refer to parallel and perpendicular polarization of the electric field to the wood fibre. Fig. 8 shows the real part of the complex permittivity with frequency for the

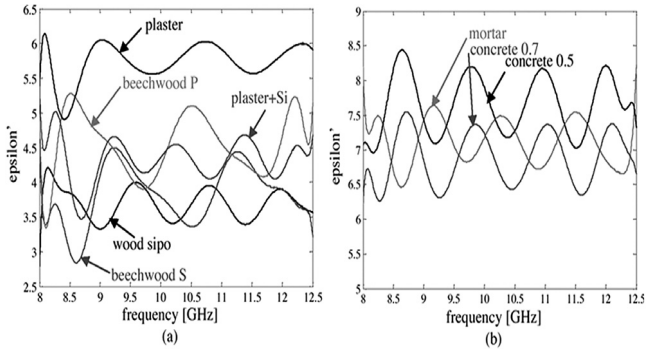

Fig. 8. Real part of permittivity: relationship with frequency [197].

Table 13
Dielectric constants for different types of material at different frequencies and polarizations [198].

	Permittivity				Conductivity			
	5.8 GHz		41.5 GHz		5.8 GHz		41.5 GHz	
	V	H	V	H	V	H	V	H
Glass	6.06	5.98	3.41	3.43	0.35	0.35	0.24	0.26
Plywood	2.88	2.87	1.69	1.77	0.21	0.16	0.52	0.54
Plasterboard	2.02	2.21	2.5	2.15	0	0	0.23	0.24
Brick	3.58	3	–	–	0.11	0.12	–	–

tested materials [197]. As seen in the figure, material permittivity behaviour with respect to frequency is not straightforward; however the general behaviour can be observed: the plaster with silica and beechwood show a slight trend for epsilon to increase with frequency, while the average value for other material remains the same, especially in the 9–12.5 GHz band. Due to greater porosity for concrete 0.7 the real part of its permittivity is than that for concrete 0.5.

The effect of polarization on permittivity and conductivity was studied by [198] for 5.8 and 41.5 GHz: a summary of their work is presented in Table 13 [198].

Due to the horizontal orientation of the brick wall, results vary between the horizontal and vertical polarization, while for other

materials no substantial difference is observed [198]. In [199], measurements were conducted at 2.4 GHz to study the permittivity for stone, concrete and glass walls. The average results were 5.4 for the concrete, 2.3 for the glass, while for indoor and outdoor stone walls the permittivities recorded were 4.5 and 7.9 respectively. The difference between the permittivities of indoor and outdoor stone walls is due to differences in the percentage of wall moisture [199]. The values for the permittivity of glass given in by [178] and [179] differ significantly: this is believed to be due to different types of glass used in the experiments.

6. Propagation through buildings

Since most cell phones spend most of the time inside buildings, the received service level inside should be above the receiver threshold level. Therefore, building penetration loss should be taken into account. Penetration losses can be classified into wall loss, room loss, floor loss and building loss [82]. Wall loss depends on the angle of incidence: as the angle approaches grazing incidence losses become greater, but they also depend on operating frequency, wall material and thickness. Hence penetration losses are different when comparing between LOS and NLOS propagation, depending on the environmental conditions. Building penetration loss (BPL) depends on the environment, antenna heights, LOS/NLOS propagation, operating frequency, the angle of incidence and on the material type [200].

6.1. Path loss exponent model with correction factors

These models were investigated by [201] and [117]. They started with a path loss exponent model: in order to characterize the propagation environment, more than one path loss exponent was used, $n_{outdoor}$ and n_{indoor} [202]. Although the simplicity of this approach is attractive, as it only requires the distance between transmitter and receiver, the signal estimation was poor. The authors used the concept of "aggregate penetration loss" APL: signal strengths were collected outside the building from different places just behind the building to avoid building shadowing. These losses were averaged and indoor signal powers were collected from different locations within the building and then averaged. The ratio between the two averages was termed as APL [203]:

$$APL = 10\log_{10}\left[\frac{\frac{1}{N}\sum_{i=1}^{N} S_i^{outdoor}}{\frac{1}{M}\sum_{j=1}^{M} S_j^{indoor}}\right] \tag{42}$$

where S, N and M are received signal strength, the number of outdoor collected measurements and number of indoor measurements respectively. The APL is added to the path loss exponent model which uses only $n_{outdoor}$; for the outdoor losses the model is used without the APL; while for indoor losses, the estimated APL value is added. It should be noted that APL is different from loss due to the exterior walls of the building [201].

Partition-based penetration (PBP) loss is defined as the loss difference between two measurements collected on the direct inside and outside of the external house wall [201]. In [201] empirical values for PBP are presented, the total losses are the sum of free space loss and the PBP losses for obstructions lying on the line of sight between transmitter and receiver. Using the nth power law for propagation leads to having a wide range of standard deviations for measurements recorded at specific locations; therefore the use of the PBP concept reduces these deviations [201]. The model works satisfactorily as long as the number of scatterers is relatively small; otherwise multipath dominates and that is not considered in this model. Another constraint on this model is that it is not valid for signal strength estimation within buildings [201].

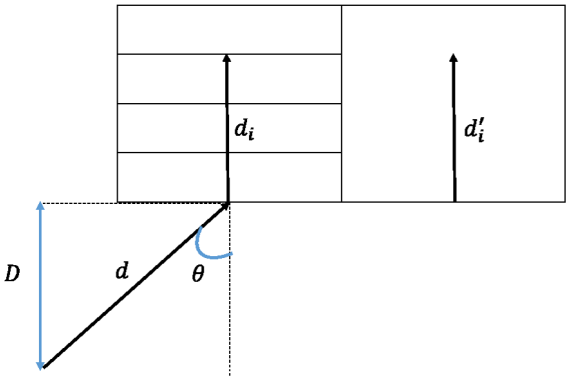

Fig. 9. COST 231 LOS BPL model.

Table 14
Typical values for $(L_e, L_g, L_i \& \alpha)$ [82].

Parameter	Material	Loss value
L_e/L_{in}	Concrete wall	7 dB
	Wood/Plaster wall	4 dB
	Residential	6.2/3
L_g	Concrete wall	20 dB
	Residential	10 dB
α	–	0.6 dB/m

6.2. COST231 building penetration studies

Extensive sets of measurements were developed by the European COST (Co-operation in the field of Scientific and Technical research) program 231. These studied outdoor to indoor propagation models, the measurements being conducted in the range of 900–1800 MHz, valid for 500 m distance between the base station and the building of interest, where the base station height is less than 30 metres [82,117]. In the case of LOS propagation, the total path loss L_T between two isotropic antennas is given by Eq. (43), where one is located outside the building and the other is located inside as shown in Fig. 9 [82]. The total losses can be considered in three categories: outdoor losses L_{out}, penetration losses L_{pen} and indoor losses L_{in}.

$$L_T = L_{out} + L_{pen} + L_{in} \tag{43}$$

where:

$$L_{out} = L_{FS} \tag{44}$$

$$L_{pen} = L_e + L_g\,(1 - \cos\theta)^2 \tag{45}$$

$$L_{in} = \max(n_w L_i, \alpha(d_i - 2)\,(1 - \cos\theta)) \tag{46}$$

where θ is the angle of incidence which is given by $\cos^{-1}(D/d)$, L_{FS} is free space path loss for path $(d_i + d)$, L_e is the external wall loss at $\theta = 0^0$, L_g is the additional external loss at $\theta = 90^0$, n_w is the number of walls, L_i is the internal wall loss, d_i' is the unobstructed path and α is the d_i' specific attenuation (dB/m). Typical values for parameters in Eq. (43)–(46) are given in Table 14.

Values of L_e and L_i range between 4–10 dB; concrete walls can increase the losses to the range of 10–20 dB in the case where the walls are without windows. Thin wood and plaster walls cause losses of less than 4 dB. Walls with larger window sizes tend to have less loss, but metallized windows tend to have larger loss [82].

In the case of NLOS propagation, the path loss is expressed in terms of an outer reference path loss at a height of 2m [82]:

$$L_{out} = L_{FS} \tag{47}$$

Table 15
Typical values for COST231 building penetration model parameters [82].

Parameter	Loss	Comments
L_{ge}	3–5	900 MHz
	5–7	1800 MHz
	7–8	2100 MHz [204]
G_n	1.5–2	900/1800 MHz, building height below 4-5 m
	4–7	900/1800 MHz, building height above 4–5 m
G_h	1.1–1.6	1800 MHz, building height above 4–5 m

$$L_{pen} = L_e + L_{ge} - G_{FH} \tag{48}$$

$$L_{in} = \max(n_w L_i, \alpha d_i) \tag{49}$$

Given that:

$$G_{FH} = n \cdot G_n \text{ or } h \cdot G_h \tag{50}$$

where is L_{ge}, n, G_n, h and G_h are tuning correction factors for L_e [117], floor number, floor height gain (dB/floor), height above the outdoor reference and height gain (dB/m). Typical values for parameters in Eqs. (48) and (50) are given in Table 15.

Shadowing fading (outdoor shadowing and indoor shadowing) tends to follow a log-normal distribution with 4–5 dB standard deviation [82].

6.3. Building penetration loss and extensions to the COST231 model

In the literature, information about the relationship between BPL and frequency are rather conflicting: while some researchers state that BPL increases as frequency increases [205–214], another group claims the opposite [93,204,215–218]. A third group claims that either no frequency dependency exists or there is an irregular frequency dependency [219,220]. Figs. 10 and 11 show a literature summary on BPL dependence on frequency.

Measurements in [220] show interesting observations: using the same set of frequencies and equipment, general BPL behaviour neither increases nor decreases with frequency, as shown in Fig. 12, which may give an explanation for the conflicting results in the literature. This suggests that frequency dependence may or may not occur, depending on the environment.

The authors in [220] proposed a formula for BPL. The aim of their work was to refine the COST 231 model. Experiments were performed in 71 floors within 17 buildings of two types (office buildings and multi-storey car parks). A wide range of frequencies was investigated (0.8, 2.2, 4.7 and 8.45 GHz). It was observed that BPL has no clear dependence on frequency: among the applied frequencies, BPL was around 10 dB and 3 dB for office buildings and multi-storey car park, respectively. It was also observed that BPL increases proportionally as the distance between the mobile station and the window of the outer wall increases.

Floor height gain G_h tends to be independent of the distance between the base station and the building and it shows no frequency dependence. It was also observed that α increases slightly as frequency increases; while it has no dependence on the distance between the base station and the building. BPL is given by Equation (51) [220]:

$$BPL = \alpha d + G_h h + \alpha_{LOS} k + \alpha_f \log f + W \tag{51}$$

where $d, h, k, \alpha_{LOS}, \alpha_f$ and W are building penetration distance, floor height, LOS constant, LOS coefficient, frequency coefficient and constant loss respectively. Typical values for Eq. (51) parameters are given in Table 16 [220].

In [210] experiments were carried out at 0.46, 0.88, 1.860 and 5.1 GHz. It was found that, in NLOS scenarios, as the height increases losses tend to decrease; little frequency dependence was observed in the range of 460–1860 MHz, although some

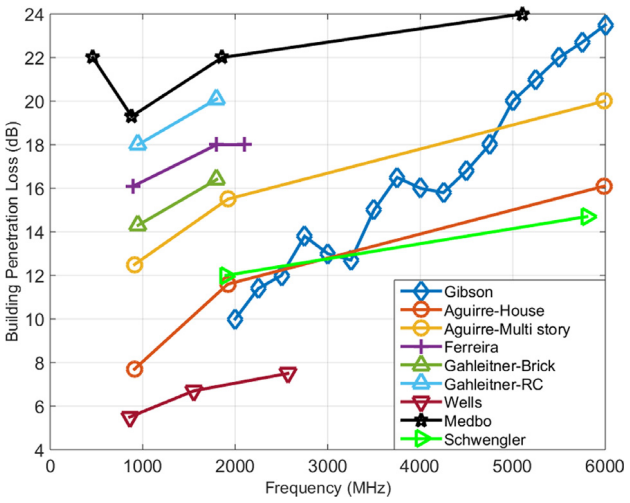

Fig. 10. BPL increasing with frequency according to many references (as cited).

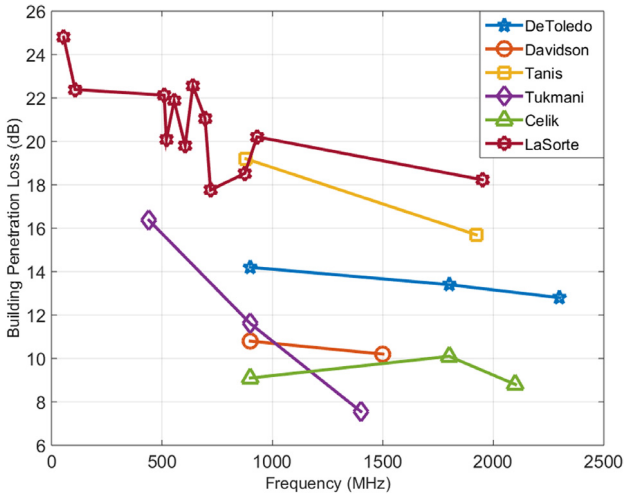

Fig. 11. BPL decreasing with frequency according to many references (cited).

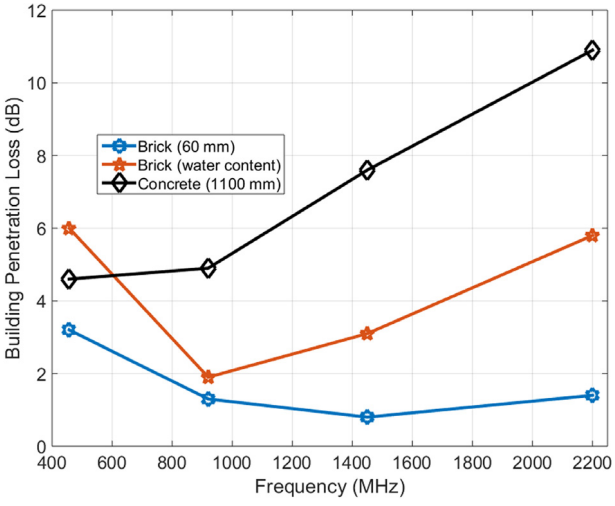

Fig. 12. BPL behaviour with frequency for different types of buildings.

Table 16
Typical values for the proposed BPL parameters.

Parameter	Comment
d	0–20 m
α	0.6 dB/m
G_h	0.6 dB/m
h	1.5–30 m
α_{LOS}	−0.8 & −3.9
α_f	−1.1
k	1: LOS 0: NLOS
W	10 dB

dependence was observed in some buildings in the range of 1.8–5.1 GHz. For this study the BPL is given by [210]:

$$L_{pen} = \frac{10}{a}\log_{10}\left[10^{\frac{G_{NLOS}a(n_{LOS}-n)}{10}} + 1\right] + L_{LOS} \quad (52)$$

where a is a tuning parameter to adjust the size of the model transition zone between LOS and NLOS conditions, n is the floor number, n_{LOS} the lowest floor number for which there is LOS towards the transmitter, G_{NLOS} is the floor gain in NLOS conditions and L_{LOS} is BPL in the LOS conditions.

In [221], the authors explored the effect of opening and closing the windows on BPL. Data were collected at distances from 0.2 to 5 m away from the wall at 1800 MHz: over this range, BPL difference between opened and closed window cases were almost the same, at around 11 dB. BPL tended to increase as signals travelled deeper into the building, and decrease when observed on higher floors in the building [207].

A study on satellite-indoor services over the band from 2 to 6.5 GHz concluded that BPL increases monotonically as the elevation angle increases in both LOS and NLOS cases [222], similar results were also obtained by [223,224]. BPL was found to be larger as the incidence angle increased towards grazing incidence [200].

Chee et al. [225] proposed an extension to the COST231 model, based on measurements carried out at 800 and 3500 MHz for seven residential buildings. The BPL observed showed no frequency dependence; in the case of walls with windows, measurements showed that a 5–6 dB reduction in the BPL value was observed, compared to the case of walls without windows. In [226], the authors proposed a modification to the COST 231 model as this assumes penetration through walls without considering the effect of windows and doors. The proposed model assumes the dominant rays are those propagating through wall openings, doors and windows. The model also includes the effect of angular dependency on penetration losses. Taking these factors into account, the termL_{pen} is updated to [226]:

$$L_{pen} = L'_e + L_g\,(1-\cos\theta)^2 + f\,(\varphi) \quad (53)$$

where L'_e is the loss across wall openings for $\theta = 90^0$ which was found to vary from 5 to 28 dB, L_g is the same as in the COST 231 model and $f\,(\varphi)$ is the angular dependency factor (φ is the angle between the refracted ray and the receiver). $f\,(\varphi)$ was found to be close to $\left(L_g \cdot \sin\varphi\right)$.

i. COST 231 Walfisch–Ikegami model:

In [227] modification of the COST 231 was proposed for LOS conditions: in this, the free space loss factor in Eq. (47) is replaced by a LOS COST 231 Walfisch–Ikegami model:

$$L_{out} = 42.6 + 26\log(D) + 20\log(f) \quad (54)$$

where D is in km, and f in MHz. The Walfisch–Ikegami model is valid over the frequency range of 0.8–2 GHz, over distances from 0.02 to 5 km and for base station heights from 4 to 50 m [82]. The other modification is a simplification for the indoor loss term which is replaced by Eq. (55) [228], provided that there is one internal wall per ten metres, this modification reduces the requirement for detailed knowledge of the position of the mobile station [229]. The model is claimed to have better performance compared to the original COST 231 model [229].

$$L_{in} = \alpha \cdot d_i \quad (55)$$

ii. Winner II model:

Another modification to the COST 231 and COST 231 WI models is the Winner II (Wireless World Initiative New Radio) [86]. The first model termed as "*Winner II B4 model*" considers the propagation through an urban microcell environment. In this, the receiver antenna heights are around 1–2 m in addition to the floor height, while the base station is at 10 m on top of surrounding buildings. The receiver building is up to 3 floors, and distance range 3–1000 m between the transmitter and receiver: the model is valid over the range of frequencies 2–6 GHz.

$$L_{out} = \max\begin{cases} 41 + 22.7\log_{10}(D+d_i) + 20\log_{10}\dfrac{f}{5} \\ L_{FS} \end{cases} \quad (56)$$

$$L_{tw} = L_e + L_g\,(1-\cos\theta)^2 \quad (57)$$

$$L_{in} = \alpha \cdot d_i \quad (58)$$

Typical values for L_e, L_g and α are 14 dB, 15 dB and 0.5 dB/m respectively. The other model is for the urban macro propagation case: this model is termed the "*Winner II C4 model*". The receiver antenna heights are around 1–2 m in addition to the floor height, while the base station is 25 m on top of surrounding buildings, the receiver building is up to 3 floors, and distances in the range 50 to 5000 m between the transmitter and receiver were considered. The model is valid over the range of frequencies 2–6 GHz and for a base station antenna which is higher than 30 m.

$$L_{out} = (44.9 - 6.55\log_{10}h_b)\log_{10}(D+d_i) + 20\log_{10}\frac{f}{5} + 5.83\log_{10}h_b + 26.46 \quad (59)$$

$$L_{tw} = L_e + hG_h \quad (60)$$

$$L_{in} = \alpha \cdot d_i \quad (61)$$

where f is in GHz and h_b is the base station height. Typical values for L_e, G_h and α respectively are 17.4 dB, 0.8 dB/m and 0.5 dB/m. It should be noted that the Winner II models are applicable only when the mobile station is above ground level, (i.e. they do not apply for negative mobile heights) [230].

Indoor to outdoor propagation and outdoor to indoor propagation are not reciprocal as might be expected. In [231] comparison between the two scenarios is presented using MIMO measurements at 5.25 GHz: the investigated parameters include the delay spread, fast fading represented by the K-factor, azimuth spread and polarization represented by cross-polarization. The study showed that the angular spread and polarization characteristics have high reciprocity while this is not necessarily true for their temporal parameters.

In a study conducted by [232], the propagation of indoor stairwell was investigated at 2.4 GHz, while the transmitter was fixed outside the building, the receiver was mounted on different stairwell steps levels, different polarization configurations were studied including VV, HH and VH. It was found that stairwell walls do not reflect much of incoming energy, while transmitted energy contributes significantly to the RSS level, hybrid rays (reflections and transmissions) was found to contribute in the SS level. In most cases, it was also found that VV polarization has the best RSS level. Due to multiple reflections from the walls and transmissions through stairs, propagation through stairwell tends to

have significant EM depolarization. In [233] authors investigated the propagation in the indoor stairwell, they found that path loss exponent tends to be higher than multi-floor environments, average PLE values are around 7–10 and 7–13 at 2.4 GHz and 5.8 GHz respectively.

7. Conclusions

A review of indoor propagation researches has been presented. This has been aimed at helping to achieve a better understanding of indoor service applications: the study explores the major differences between outdoor and indoor propagation and provides current frequency allocations for many indoor applications. Channel modelling, including stochastic and deterministic approaches, has been introduced: in the stochastic modelling different channel parameters including signal strength, power delay, coherence bandwidth, Doppler spread, the angle of arrival have been explored and major channel attributes like path loss, shadowing and fast fading mechanisms are further investigated. The concept of MIMO channels is also covered. In the field of deterministic channel modelling, many methods are presented, including Finite Difference Time Domain method, Finite Integration Method, Ray tracing and the Dominant path model. Building material properties with frequency have also been investigated with a comparison of current research outcomes. Many models for propagation through buildings, including COST 231 and its extensions, and WINNER II are introduced and compared.

Declaration of competing interest

The authors declare that they have no known competing financial interests or personal relationships that could have appeared to influence the work reported in this paper.

References

[1] A. Goldsmith, Wireless Communications, Cambridge university press, 2005.

[2] G.L. Turin, F.D. Clapp, T.L. Johnston, S.B. Fine, D. Lavry, A statistical model of urban multipath propagation, IEEE Trans. Veh. Technol. 21 (1) (1972) 1–9.

[3] A. Yassin, et al., Recent advances in indoor localization: A survey on theoretical approaches and applications, IEEE Commun. Surv. Tutor. (2016).

[4] H.A. Obeidat, et al., A comparison between vector algorithm and CRSS algorithms for indoor localization using received signal strength, in: The Applied Computational Electromagnetics Society (ACES), Vol. 31, 2016, pp. 868–876.

[5] M. Tolstrup, Indoor Radio Planning: A Practical Guide for 2G, 3G and 4G, John Wiley & Sons, 2015.

[6] N. Blaunstein, C. Christodoulou, Indoor radio propagation, in: Radio Propagation and Adaptive Antennas for Wireless Communication Links: Terrestrial, Atmospheric and Ionospheric, 2014, pp. 302–334.

[7] Z. Zhang, X. Di, J. Tian, P. Chen, A WLAN planning method for indoor positioning system, in: 2016 International Conference on Information Networking (ICOIN), IEEE, 2016, pp. 303–307.

[8] J. Lloret, J.J. López, C. Turró, S. Flores, A fast design model for indoor radio coverage in the 2.4 GHz wireless LAN, in: 1st International Symposium on Wireless Communication Systems, IEEE, Mauritius, Mauritius, 2004, pp. 408–412.

[9] A. Ahmad, M.M. Rathore, A. Paul, W.-H. Hong, H. Seo, Context-aware mobile sensors for sensing discrete events in smart environment, J. Sensors 2016.

[10] K.-H. Park, et al., Robotic smart house to assist people with movement disabilities, Auton. Robots 22 (2) (2007) 183–198.

[11] S. Amendola, R. Lodato, S. Manzari, C. Occhiuzzi, G. Marrocco, RFID technology for IoT-based personal healthcare in smart spaces, IEEE Internet Things J. 1 (2) (2014) 144–152.

[12] N. Chowdhary, S. Kaur, S. Mahajan, Study and analysis of LTE-advanced systems at 2.6 GHz for indoor large hall, 2016.

[13] Z. Cao, X. Zhao, F.M. Soares, N. Tessema, T. Koonen, 38-GHz millimeter wave beam steered fiber wireless systems for 5G indoor coverage: Architectures, devices and links, IEEE J. Quantum Electron. (2016).

[14] S. Chen, J. Zhao, The requirements, challenges, and technologies for 5G of terrestrial mobile telecommunication, IEEE Commun. Mag. 52 (5) (2014) 36–43.

[15] P. Chai, L. Zhang, Indoor radio propagation models and wireless network planning, in: Computer Science and Automation Engineering (CSAE), 2012 IEEE International Conference on, Vol. 2, IEEE, 2012, pp. 738–741.

[16] H. Hashemi, The indoor radio propagation channel, Proc. IEEE 81 (7) (1993) 943–968.

[17] S. Saunders, A. Aragón-Zavala, Antennas and Propagation for Wireless Communication Systems: 2nd Edition, John Wiley & Sons, 2007.

[18] M. Sheikhsofla, K. Sarabandi, Indoor wave propagation simulations at HF using rayleigh-gans approximation, in: 2013 USNC-URSI, Radio Science Meeting (Joint with AP-S Symposium), IEEE, 2013, p. 202.

[19] Y. Zhu, et al., Demystifying 60 GHz outdoor picocells, in: Proceedings of the 20th Annual International Conference on Mobile Computing and Networking, 2014, pp. 5–16.

[20] S. Kutty, D. Sen, An improved numerical optimization method for efficient beam search in 60 GHz indoor millimeter wave wireless networks, in: 2015 IEEE International Conference on Advanced Networks and Telecommuncations Systems, IEEE, 2015, pp. 1–6.

[21] C. Alippi, M. Bocca, G. Boracchi, N. Patwari, M. Roveri, RTI goes wild: Radio tomographic imaging for outdoor people detection and localization, IEEE Trans. Mob. Comput. 15 (10) (2016) 2585–2598.

[22] S. Sun, G.R. MacCartney, T.S. Rappaport, Millimeter-wave distance-dependent large-scale propagation measurements and path loss models for outdoor and indoor 5G systems, in: 2016 10th European Conference on Antennas and Propagation (EuCAP), IEEE, 2016, pp. 1–5.

[23] K.R. Foster, J.E. Moulder, Wi-Fi and health: review of current status of research, Health Phys. 105 (6) (2013) 561–575.

[24] T.S. Rappaort, Wireless Communications: Principles and Practice, second ed., Prentice Hall, Upper Saddle River, NJ, USA, 2002.

[25] A. Aragón-Zavala, Indoor Wireless Communications: From Theory to Implementation, John Wiley & Sons, 2017.

[26] M.K. Awad, K.T. Wong, Z.-b. Li, An integrated overview of the open literature's empirical data on the indoor radiowave channel's delay properties, IEEE Trans. Antennas and Propagation 56 (5) (2008) 1451–1468.

[27] C. Gandarillas, V. Iglesias, M. Aparicio, E. Mino-Díaz, P. Olmos, A new approach for improving indoor LTE coverage, in: 2011 IEEE GLOBECOM Workshops (GC Wkshps), IEEE, 2011, pp. 1330–1335.

[28] H. Fukudome, K. Akimoto, S. Kameda, N. Suematsu, T. Takagi, K. Tsubouchi, Measurement of 3.5 GHz band small cell indoor-outdoor propagation in multiple environments, in: European Wireless 2016; 22th European Wireless Conference, VDE, 2016, pp. 1–6.

[29] S.K. Saha, A. Garg, D. Koutsonikolas, A first look at TCP performance in indoor IEEE 802.11 ad WLANs, in: 2015 IEEE Conference on Computer Communications Workshops (INFOCOM WKSHPS), IEEE, 2015, pp. 63–64.

[30] N. Qadar, et al., Investigating the effects of microwave oven on the performance of Wi-Fi network, in: 2014 12th International Conference on Frontiers of Information Technology (FIT), IEEE, 2014, pp. 34–36.

[31] M.K. Samimi, T.S. Rappaport, Characterization of the 28 GHz Millimeter-Wave Dense Urban Channel for Future 5G Mobile Cellular, Technical Report, TR 2014-001, 2014.

[32] R. Mautz, Indoor positioning technologies, in: Habilitationsschrift, ETH Zürich, 2012.

[33] M. Lei, et al., 28-GHz indoor channel measurements and analysis of propagation characteristics, in: 2014 IEEE 25th Annual International Symposium on Personal, Indoor, and Mobile Radio Communication (PIMRC), IEEE, 2014, pp. 208–212.

[34] M.-D. Kim, J. Liang, J. Lee, J. Park, B. Park, Path loss measurements and modeling for indoor office scenario at 28 and 38 GHz, in: 2016 International Symposium on Antennas and Propagation (ISAP), IEEE, 2016, pp. 64–65.

[35] M. Bocquet, C. Loyez, M. Fryziel, N. Rolland, Millimeter-wave broadband positioning system for indoor applications, in: 2012 IEEE MTT-S International Microwave Symposium Digest (MTT), 2012, pp. 1–3.

[36] C. Loyez, N. Rolland, M. Bocquet, UWB technology applied to millimeter-wave indoor location systems, in: 2014 International Radar Conference (Radar), IEEE, 2014, pp. 1–5.

[37] S. Zvanovec, P. Pechac, M. Klepal, Wireless LAN networks design: site survey or propagation modeling? Radioengineering 12 (4) (2003) 42–49.

[38] A. Alhamoud, et al., Empirical investigation of the effect of the door's state on received signal strength in indoor environments at 2.4 GHz, in: 39th Annual IEEE Conference on Local Computer Networks Workshops, IEEE, 2014, pp. 652–657.

[39] Wireless InSite Reference Manual, 3.1.0 ed., REMCOM, State College, Pennsylvania, 2017.

[40] J.B. Andersen, T.S. Rappaport, S. Yoshida, Propagation measurements and models for wireless communications channels, IEEE Commun. Mag. 33 (1) (1995) 42–49.

[41] T.S. Rappaport, S.Y. Seidel, K. Takamizawa, Statistical channel impulse response models for factory and open plan building radio communicate system design, IEEE Trans. Commun. 39 (5) (1991) 794–807.

[42] S.Y. Seidel, T.S. Rappaport, 914 MHz path loss prediction models for indoor wireless communications in multifloored buildings, IEEE Trans. Antennas and Propagation 40 (2) (1992) 207–217.

[43] S.S. Ghassemzadeh, R. Jana, C.W. Rice, W. Turin, V. Tarokh, Measurement and modeling of an ultra-wide bandwidth indoor channel, IEEE Trans. Commun. 52 (10) (2004) 1786–1796.

[44] P. Njemcevic, A novel approach in determination of the appropriate spatial averaging signal length, Wirel. Pers. Commun. 82 (3) (2015) 1851–1861.

[45] R.A. Valenzuela, O. Landron, D. Jacobs, Estimating local mean signal strength of indoor multipath propagation, IEEE Trans. Veh. Technol. 46 (1) (1997) 203–212.

[46] A.C. Austin, Wireless channel characterization in burning buildings over 100–1000 MHz, IEEE Trans. Antennas and Propagation 64 (7) (2016) 3265–3269.

[47] A.C. Austin, N. Sood, J. Siu, C.D. Sarris, Application of polynomial chaos to quantify uncertainty in deterministic channel models, IEEE Trans. Antennas and Propagation 61 (11) (2013) 5754–5761.

[48] A. Austin, Performance estimation for indoor wireless systems using FDTD method, Electron. Lett. 51 (17) (2015) 1376–1378.

[49] A.C.M. Austin, M.J. Neve, G.B. Rowe, Modeling propagation in multifloor buildings using the FDTD method, IEEE Trans. Antennas and Propagation 59 (11) (2011) 4239–4246.

[50] M. Lindhé, K.H. Johansson, A. Bicchi, An experimental study of exploiting multipath fading for robot communications, in: 3rd International Conference on Robotics Science and Systems, RSS 2007, 27–30 June 2007, Atlanta, GA, USA, 2008, pp. 289–296.

[51] P. Njemčević, A. Lipovac, V. Lipovac, Improved model for estimation of spatial averaging path length, Wirel. Commun. Mobile Comput. (2018).

[52] W.C. Lee, Estimate of local average power of a mobile radio signal, IEEE Trans. Veh. Technol. 34 (1) (1985) 22–27.

[53] D. de la Vega, et al., Generalization of the lee method for the analysis of the signal variability, IEEE Trans. Veh. Technol. 58 (2) (2009) 506–516.

[54] N. Pamela, Local average signal estimation in nakagami-m channels, in: 2014 6th International Symposium on Communications, Control and Signal Processing (ISCCSP), IEEE, 2014, pp. 441–444.

[55] J. Seseña Osorio, I. Zaldivar-Huerta, A. Aragón-Zavala, Experimental estimation of the large-scale fading in an indoor environment and its impact on the planning of wireless networks, in: 2013 SBMO/IEEE MTT-S International Microwave & Optoelectronics Conference (IMOC), IEEE, 2013, pp. 1–5.

[56] S.S. Zhekov, O. Franek, G.F. Pedersen, Numerical modeling of indoor propagation using FDTD method with spatial averaging, IEEE Trans. Veh. Technol. 67 (9) (2018) 7984–7993.

[57] G. Retscher, T. Tatschl, Indoor positioning using wi-fi lateration—Comparison of two common range conversion models with two novel differential approaches, in: Fourth International Conference on Ubiquitous Positioning, Indoor Navigation and Location Based Services (UPINLBS), IEEE, 2016, pp. 1–10.

[58] S. Zvanovec, M. Valek, P. Pechac, Results of indoor propagation measurement campaign for WLAN systems operating in 2.4 GHz ISM band, in: Twelfth International Conference on Antennas and Propagation, (ICAP 2003), Vol. 1, IET, Exeter, UK, 2003, pp. 63–66.

[59] S. Alexander, G. Pugliese, Cordless communication within buildings: Results of measurements at 900 MHz and 60 GHz, Br. Telecommun. Technol. J. 1 (1) (1983) 99–105.

[60] R. Davies, A. Simpson, J. Mcgreehan, Propagation measurements at 1.7 GHz for microcellular urban communications, Electron. Lett. 26 (14) (1990) 1053–1055.

[61] J.A. Dabin, N. Ni, A.M. Haimovich, E. Niver, H. Grebel, The effects of antenna directivity on path loss and multipath propagation in UWB indoor wireless channels, in: IEEE Conference on Ultra Wideband Systems and Technologies, IEEE, 2003, pp. 305–309.

[62] S. Phaiboon, An empirically based path loss model for indoor wireless channels in laboratory building, in: 2002 IEEE Region 10 Conference on Computers, Communications, Control and Power Engineering. TENCOM'02. Proceedings, Vol. 2, IEEE, 2002, pp. 1020–1023.

[63] G.J. Janssen, R. Prasad, Propagation measurements in an indoor radio environment at 2.4 GHz, 4.75 GHz and 11.5 GHz, in: [1992 Proceedings] Vehicular Technology Society 42nd VTS Conference-Frontiers of Technology, IEEE, 1992, pp. 617–620.

[64] A. Muqaibel, A. Safaai-Jazi, A. Attiya, B. Woerner, S. Riad, Path-loss and time dispersion parameters for indoor UWB propagation, IEEE Trans. Wireless Commun. 5 (3) (2006) 550–559.

[65] S. Deng, M.K. Samimi, T.S. Rappaport, 28 GHz and 73 GHz millimeter-wave indoor propagation measurements and path loss models, in: 2015 IEEE International Conference on Communication Workshop, IEEE, 2015, pp. 1244–1250.

[66] S.S. Ghassemzadeh, R. Jana, C.W. Rice, W. Turin, V. Tarokh, A statistical path loss model for in-home UWB channels, in: 2002 IEEE Conference on Ultra Wideband Systems and Technologies (IEEE Cat. No. 02EX580), IEEE, 2002, pp. 59–64.

[67] D. Devasirvathan, Multi-frequency propagation measurements and models in a large metropolitan commercial building for personal communications, in: IEEE International Symposium on Personal, Indoor and Mobile Radio Communications, IEEE, UK, 1991, pp. 98–103.

[68] P. Karlsson, Indoor Radio Propagation for Personal Communications Services (PhD diss.), Lund Institute of Technology, 1995.

[69] K. Cheung, J. Sau, M. Fong, R.D. Murch, Indoor propagation prediction utilizing a new empirical model, in: Proceedings Conference Singapore ICCS'94, Vol. 1, IEEE, 1994, pp. 15–19.

[70] C.B. Andrade, R.P.F. Hoefel, IEEE 802.11 WLANs: A comparison on indoor coverage models, in: 2010 23rd Canadian Conference on Electrical and Computer Engineering (CCECE), IEEE, Calgary, AB, Canada, 2010, pp. 1–6.

[71] K. Nuangwongsa, et al., Path loss modeling in durian orchard for wireless network at 5.8 GHz, in: 2009 6th International Conference on Electrical Engineering/Electronics, Computer, Telecommunications and Information Technology, Vol. 2, IEEE, Pattaya, Chonburi, Thailand, 2009, pp. 816–819.

[72] Y. Zhao, M. Li, F. Shi, Indoor radio propagation model based on dominant path, Int. J. Commun. Netw. Syst. Sci. 3 (3) (2010) 330.

[73] Z. Jiang, J. Yu, R. Zhu, K. Yang, W. Chen, Experimental multipath delay spread and path loss analysis for the indoor environment at 5.9 GHz, in: International Conference on Wireless Communications, Signal Processing and Networking (WiSPNET), IEEE, 2016, pp. 1859–1863.

[74] I.T.U. ITU, Propagation data and prediction methods for the planning of indoor radiocommunication systems and radio local area networks in the frequency range 900 MHz to 100 GHz, in: Recommendation ITU-R P.1238-7, ITU, ed. Geneva, 2012.

[75] J. Keenan, A. Motley, Radio coverage in buildings, Br. Telecommun. Technol. J. 8 (1) (1990) 19–24.

[76] A.G. Lima, L.F. Menezes, Motley-keenan model adjusted to the thickness of the wall, in: SBMO/IEEE MTT-S International Conference on Microwave and Optoelectronics, IEEE, Brasilia, Brazil, 2005, pp. 180–182.

[77] N. Sah, N.R. Prakash, A. Kumar, D. Kumar, D. Kumar, Optimizing the path loss of wireless indoor propagation models using CSP algorithms, in: 2010 Second International Conference on Computer and Network Technology (ICCNT), 2010, pp. 324–328.

[78] K. Sayidmarie, A.H. Aboud, M.S. Salim, Estimation of wall penetration loss for indoor WLAN systems, in: 2012 6th International Conference on Sciences of Electronics, Technologies of Information and Telecommunications (SETIT), 2012, pp. 675–679.

[79] J.-F. Lafortune, M. Lecours, Measurement and modeling of propagation losses in a building at 900 MHz, IEEE Trans. Veh. Technol. 39 (2) (1990) 101–108.

[80] G.R. Maccartney, T.S. Rappaport, S. Sun, S. Deng, Indoor office wideband millimeter-wave propagation measurements and channel models at 28 and 73 GHz for ultra-dense 5G wireless networks, IEEE Access 3 (2015) 2388–2424.

[81] A. Motley, J. Keenan, Personal communication radio coverage in buildings at 900 MHz and 1700 MHz, Electron. Lett. 24 (12) (1988) 763–764.

[82] G.F. Pedersen, COST 231-Digital Mobile Radio Towards Future Generation Systems, European Commission, 1999.

[83] S.Y. Seidel, et al., The impact of surrounding buildings on propagation for wireless in-building personal communications system design, in: [1992 Proceedings] Vehicular Technology Society 42nd VTS Conference-Frontiers of Technology, IEEE, 1992, pp. 814–818.

[84] C. Serôdio, et al., A lightweight indoor localization model based on motley-keenan and cost, in: Proceedings of the World Congress on Engineering, Vol. 2, International Association of Engineers, London, UK, 2012, pp. 1323–1328.

[85] H. Obeidat, et al., An indoor path loss prediction model using wall correction factors for WLAN and 5G indoor networks, Radio Sci. (2018).

[86] J. Meinilä, P. Kyösti, T. Jämsä, L. Hentilä, WINNER II channel models, in: Radio Technologies and Concepts for IMT-Advanced, 2009, pp. 39–92.

[87] H. Chaibi, M. Belkasmi, Z. Mohammadi, UWB outdoor channel characterization and modeling based on measurements, in: 2015 International Conference on Wireless Networks and Mobile Communications (WINCOM), 2015, pp. 1–5.

[88] C. Perez-Vega, J. Garcia, Frequency behavior of a power-law path loss model, in: Proc. 10th Microcoll. Budapest, 1999, pp. 413–416.

[89] R. Cepeda, et al., On the measurement and simulations of the frequency dependent path loss and MB-OFDM, in: 2009 IEEE International Conference on Ultra-Wideband, 2009, pp. 321–325.

[90] P. Pajusco, P. Pagani, Frequency dependence of the UWB indoor propagation channel, in: The Second European Conference on Antennas and Propagation, 2007, pp. 1–7.

[91] Y. Wang, et al., An empirical path loss model in the indoor stairwell at 2.6 GHz, in: 2014 IEEE International Wireless Symposium (IWS), IEEE, 2014, pp. 1–4.

[92] A.A. Saleh, R.A. Valenzuela, A statistical model for indoor multipath propagation, IEEE J. Sel. Areas Commun. 5 (2) (1987) 128–137.
[93] A. Turkmani, A. De Toledo, Radio transmission at 1800 MHz into, and within, multistory buildings, in: IEE Proceedings I Communications, Speech and Vision, Vol. 138, IET, 1991, pp. 577–584, no. 6.
[94] I. Dey, G.G. Messier, S. Magierowski, Joint fading and shadowing model for large office indoor WLAN environments, IEEE Trans. Antennas and Propagation 62 (4) (2014) 2209–2222.
[95] R. Bultitude, Measurement, characterization and modeling of indoor 800/900 MHz radio channels for digital communications, IEEE Commun. Mag. 25 (6) (1987) 5–12.
[96] N.A. Alsindi, B. Alavi, K. Pahlavan, Measurement and modeling of ultrawideband TOA-based ranging in indoor multipath environments, IEEE Trans. Veh. Technol. 58 (3) (2009) 1046–1058.
[97] H. Hashemi, Impulse response modeling of indoor radio propagation channels, IEEE J. Sel. Areas Commun. 11 (7) (1993) 967–978.
[98] M. Molina-Garcia, A. Fernandez-Duran, J.I. Alonso, Application of extreme value distribution to model propagation fading in indoor mobile radio environments, in: Radio and Wireless Symposium, IEEE, 2008, pp. 97–100.
[99] N.R. Diaz, J.E.J. Esquitino, Wideband channel characterization for wireless communications inside a short haul aircraft, in: Vehicular Technology Conference, 2004. VTC 2004-Spring. 2004 IEEE 59th, Vol. 1, 2004, pp. 223–228.
[100] G. Eluma, K. Arshad, Indoor statistical channel modelling using agilent 8960, in: 2013 International Conference on Current Trends in Information Technology (CTIT), 2013, pp. 265–269.
[101] L. Jiang, S.Y. Tan, Geometrically based statistical channel models for outdoor and indoor propagation environments, IEEE Trans. Veh. Technol. 56 (6) (2007) 3587–3593.
[102] H. Hashemi, D. Tholl, Statistical modeling and simulation of the RMS delay spread of indoor radio propagation channels, IEEE Trans. Veh. Technol. 43 (1) (1994) 110–120.
[103] H. Suzuki, A statistical model for urban radio propogation, IEEE Trans. Commun. 25 (7) (1977) 673–680.
[104] H. Hashemi, M. McGuire, T. Vlasschaert, D. Tholl, Measurements and modeling of temporal variations of the indoor radio propagation channel, IEEE Trans. Veh. Technol. 43 (3) (1994) 733–737.
[105] V. Bhaskar, P.A. Devi, Performance of multiband orthogonal frequency division multiplexing network in ultra wideband channels incorporating people shadowing and channel fading, IET Commun. 7 (15) (2013) 1665–1675.
[106] A. Meijerink, A.F. Molisch, On the physical interpretation of the saleh-valenzuela model and the definition of its power delay profiles, IEEE Trans. Antennas and Propagation 62 (9) (2014) 4780–4793.
[107] A.S. Poon, M. Ho, Indoor multiple-antenna channel characterization from 2 to 8 GHz, in: IEEE International Conference on Communications, IEEE, 2003, pp. 3519–3523.
[108] C.-C. Chong, C.-M. Tan, D.I. Laurenson, S. McLaughlin, M.A. Beach, A.R. Nix, A new statistical wideband spatio-temporal channel model for 5-GHz band WLAN systems, IEEE J. Sel. Areas Commun. 21 (2) (2003) 139–150.
[109] A.F. Molisch, et al., A comprehensive standardized model for ultrawideband propagation channels, IEEE Trans. Antennas and Propagation 54 (11) (2006) 3151–3166.
[110] S. Yong, Tg3c channel modeling sub-committee final report, in: IEEE802. 15-07-0584-00-003c, 2007.
[111] Q.H. Spencer, B.D. Jeffs, M.A. Jensen, A.L. Swindlehurst, Modeling the statistical time and angle of arrival characteristics of an indoor multipath channel, IEEE J. Sel. Areas Commun. 18 (3) (2000) 347–360.
[112] A. Maltsev, A. Sadri, R. Maslennikov, A. Davydov, A. Khoryaev, Channel modeling for 60 GHz WLAN systems, IEEE 802 (2008) 802.11–08.
[113] C. Gustafson, K. Haneda, S. Wyne, F. Tufvesson, On mm-wave multipath clustering and channel modeling, IEEE Trans. Antennas and Propagation 62 (3) (2014) 1445–1455.
[114] H. Hashemi, D. Tholl, Analysis of the RMS delay spread of indoor radio propagation channels, in: [Conference Record] SUPERCOMM/ICC'92 Discovering a New World of Communications, Vol. 2, IEEE, 1992, pp. 875–881.
[115] Y. Wang, W.-J. Lu, H.-B. Zhu, Propagation characteristics of the LTE indoor radio channel with persons at 2.6 GHz, IEEE Antennas Wirel. Propag. Lett. 12 (2013) 991–994.
[116] P. Karlsson, L. Olsson, Time dispersion measurement system for radio propagation at 1800 MHz and results from typical indoor environments, in: Proceedings of IEEE Vehicular Technology Conference (VTC), Vol. 3, IEEE, 1994, pp. 1793–1797.
[117] G. De la Roche, A. Alayón-Glazunov, B. Allen, LTE-Advanced and Next Generation Wireless Networks: Channel Modelling and Propagation, John Wiley & Sons, 2012.
[118] P. Nobles, D. Ashworth, F. Halsall, Propagation measurements in an indoor radio environment at 2, 5 and 17 GHz, in: IEE Colloquium on High Bit Rate UHF/SHF Channel Sounders-Technology and Measurement, IET, London, UK, 1993, pp. 4/1–4/6.
[119] A. Affandi, G. El Zein, J. Citerne, Investigation on frequency dependence of indoor radio propagation parameters, in: Gateway to 21st Century Communications Village. VTC 1999-Fall. IEEE VTS 50th Vehicular Technology Conference (Cat. No. 99CH36324), Vol. 4, IEEE, 1999, pp. 1988–1992.
[120] D. Lu, D. Rutledge, Investigation of indoor radio channels from 2.4 GHz to 24 GHz, in: IEEE Antennas and Propagation Society International Symposium, Vol. 2, IEEE, 2003, pp. 134–137.
[121] M.R. Pakravan, M. Kavehrad, H. Hashemi, Effects of rotation on the path loss and the delay spread in indoor infrared channel, in: ICC'981998 IEEE International Conference on Communications. Conference Record. Vol. 2, IEEE, 1998, pp. 817–820.
[122] C.M.P. Ho, T.S. Rappaport, Effects of antenna polarization and beam pattern on multipath delay spread and path loss in indoor obstructed wireless channels, in: 1st International Conference on Universal Personal Communications, IEEE, 1992, pp. 92–96.
[123] K. Takamizawa, S. Seidel, T. Rappaport, Indoor radio channel models for manufacturing environments, in: Proceedings. IEEE Energy and Information Technologies in the Southeast, IEEE, 1989, pp. 750–754.
[124] G. Heidari-Bateni, C.D. McGillem, Performance limitations of the indoor radio channel, in: IEEE International Symposium on Personal, Indoor and Mobile Radio Communications, IEEE, 1991, pp. 80–85.
[125] T.S. Rappaport, C.D. McGillem, UHF Fading in factories, IEEE J. Sel. Areas Commun. 7 (1) (1989) 40–48.
[126] H. Hashemi, D. Lee, D. Ehman, Statistical modeling of the indoor radio propagation channel. II, in: [1992 Proceedings] Vehicular Technology Society 42nd VTS Conference-Frontiers of Technology, IEEE, 1992, pp. 839–843.
[127] D. Nikonov, G. Kurizki, Y. Rostovtsev, The Wiley Encyclopedia of Electrical and Electronics Engineering, ed: Wiley, New York, 1999.
[128] F. Quitin, C. Oestges, F. Horlin, P. De Doncker, Polarization measurements and modeling in indoor NLOS environments, IEEE Trans. Wireless Commun. 9 (1) (2010) 21–25.
[129] J.S. Seybold, Introduction to RF Propagation, John Wiley & Sons, 2005.
[130] T.S. Rappaport, D.A. Hawbaker, Wide-band microwave propagation parameters using circular and linear polarized antennas for indoor wireless channels, IEEE Trans. Commun. 40 (2) (1992) 240–245.
[131] T.S. Rappaport, D.A. Hawbaker, Effects of circular and linear polarized antennas on wideband propagation parameters in indoor radio channels, in: Proc. Global Telecommun. Conf. Countdown to the New Millennium. Featuring a Mini-Theme on: Personal Commun. Services, Vol. 2, 1991, pp. 1287–1291.
[132] J.-M. Molina-Garcia-Pardo, J.-V. Rodríguez, L. Juan-Llacer, Polarized indoor MIMO channel measurements at 2.45 GHz, IEEE Trans. Antennas and Propagation 56 (12) (2008) 3818–3828.
[133] S. Loredo, R.P. Torres, An experimental analysis of the advantages of polarization diversity in indoor scenarios at 1.8 and 2.5 ghz, Microw. Opt. Technol. Lett. 31 (5) (2001) 355–361.
[134] X. Zhao, S. Geng, L. Vuokko, J. Kivinen, P. Vainikainen, Polarization behaviours at 2, 5 and 60 GHz for indoor mobile communications, Wirel. Pers. Commun. 27 (2) (2003) 99–115.
[135] L. Jiang, L. Thiele, A. Brylka, S. Jaeckel, V. Jungnickel, Polarization characteristics of multiple-input multiple-output channels, in: 2008 IEEE 19th International Symposium on Personal, Indoor and Mobile Radio Communications, IEEE, 2008, pp. 1–5.
[136] K. Yu, B. Ottersten, Models for MIMO propagation channels: a review, Wirel. Commun. Mobile Comput. 2 (7) (2002) 653–666.
[137] P. Almers, et al., Survey of channel and radio propagation models for wireless MIMO systems, EURASIP J. Wireless Commun. Networking 2007 (1) (2007) 56.
[138] E. Vinogradov, W. Joseph, C. Oestges, MIMO indoor propagation: A geometry-based model including time-variant fading statistics, in: 2016 10th European Conference on Antennas and Propagation (EuCAP), IEEE, 2016, pp. 1–4.
[139] J.O. Nielsen, J.B. Andersen, G. Bauch, M. Herdin, Relationship between capacity and pathloss for indoor MIMO channels, in: 2006 IEEE 17th International Symposium on Personal, Indoor and Mobile Radio Communications, IEEE, 2006, pp. 1–5.
[140] Y. Yu, et al., Measurement and empirical modeling of massive MIMO channel matrix in real indoor environment, in: 2016 8th International Conference on Wireless Communications & Signal Processing (WCSP), IEEE, 2016, pp. 1–5.
[141] P. Almers, et al., Survey of channel and radio propagation models for wireless MIMO systems, EURASIP J. Wireless Commun. Networking 2007 (1) (2007) 019070.
[142] L. Wood, W.S. Hodgkiss, Understanding the weichselberger model: A detailed investigation, in: In MILCOM 2008-2008 IEEE Military Communications Conference, IEEE, 2008, pp. 1–7.
[143] X. Zhao, S. Li, X. Liang, Q. Wang, L. Hentilä, J. Meinilä, Measurements and modelling for d2d indoor wideband MIMO radio channels at 5 GHz, IET Commun. 10 (14) (2016) 1839–1845.

[144] Y. Wang, S. Safavi-Naeini, S.K. Chaudhuri, A hybrid technique based on combining ray tracing and FDTD methods for site-specific modeling of indoor radio wave propagation, IEEE Trans. Antennas and Propagation 48 (5) (2000) 743–754.

[145] G. Wölfle, et al., Dominant path prediction model for indoor scenarios, in: German Microwave Conference (GeMIC), Vol. 27, Ulm, 2005.

[146] P. Zakharov, et al., Finite integration technique capabilities for indoor propagation prediction, in: 2009 Loughborough Antennas & Propagation Conference, IEEE, 2009, pp. 369–372.

[147] K.A. Remley, R. Anderson, A. Weisshar, Improving the accuracy of ray-tracing techniques for indoor propagation modeling, IEEE Trans. Veh. Technol. 49 (6) (2000) 2350–2358.

[148] B. Gschwendtner, G. Wölfle, B. Burk, F. Landstorfer, Ray tracing vs. ray launching in 3-d microcell modelling, 1995.

[149] M.C. Lawton, J. McGeehan, The application of a deterministic ray launching algorithm for the prediction of radio channel characteristics in small-cell environments, IEEE Trans. Veh. Technol. 43 (4) (1994) 955–969.

[150] B. Lee, A. Nix, J. McGeehan, Indoor space–time propagation modelling using a ray launching technique, in: 11th International Conference on Antennas and Propagation (ICAP 2001), Vol. 1, IET, 2001, pp. 279–283.

[151] G. Athanasiadou, A. Nix, J. McGeehan, A ray tracing algorithm for microcellular and indoor propagation modelling, in: Ninth International Conference on Antennas and Propagation, 1995. (Conf. Publ. No. 407), Vol. 2, IET, 1995, pp. 231–235.

[152] S. Loredo, L. Valle, R.P. Torres, Accuracy analysis of GO/UTD radio-channel modeling in indoor scenarios at 1.8 and 2.5 GHz, IEEE Antennas Propag. Mag. 43 (5) (2001) 37–51.

[153] Y. Dama, et al., MIMO indoor propagation prediction using 3D shoot-and-bounce ray (SBR) tracing technique for 2.4 GHz and 5 GHz, in: Proceedings of the 5th European Conference on Antennas and Propagation (EUCAP), IEEE, 2011, pp. 1655–1658.

[154] Z. Yun, M.F. Iskander, Ray tracing for radio propagation modeling: principles and applications, IEEE Access 3 (2015) 1089–1100.

[155] Z.-Y. Liu, et al., Sensitivity of power and RMS delay spread predictions of a 3D indoor ray tracing model, Opt. Express 24 (12) (2016) 13179–13193.

[156] Remcom, Wireless Insite, 2017, [Online]. Available: http://www.remcom.com/wireless-insite. (accessed: May. 23, 2019).

[157] A. HyperWorks, WinProp, 2017, [Online]. Available: http://www.altairhyperworks.com/product/FEKO/WinProp-Propagation-Modeling. (accessed: May. 23, 2019).

[158] E. Wireless, EDX Signal Pro, 2017, [Online]. Available: http://edx.com/products/indoor/. (accessed: May. 23, 2019).

[159] iBWAVE, IBWAVE Wi-Fi, 2018, [Online]. Available: http://www.ibwave.com/ibwave-wi-fi. (accessed: May. 23, 2019).

[160] Y.-K. Yoon, M.-W. Jung, J. Kim, Intelligent ray tracing for the propagaiton prediction, in: Proceedings of the 2012 IEEE International Symposium on Antennas and Propagation, IEEE, 2012, pp. 1–2.

[161] A. Communications, Indoor ray optical propagation models, highly accurate ray optical prediction models, 2016, [Online]. Available: http://awe-communications.com/Propagation/Indoor/RayOptical/index.htm. (accessed: May. 23, 2019).

[162] Z. Lai, et al., Intelligent ray launching algorithm for indoor scenarios, Radioengineering (2011).

[163] D.M. Pozar, Microwave Engineering, John Wiley & Sons, 2012.

[164] L. Nagy, R. Dady, A. Farkasvolgyi, Algorithmic complexity of FDTD and ray tracing method for indoor propagation modelling, in: 2009 3rd European Conference on Antennas and Propagation, IEEE, 2009, pp. 2262–2265.

[165] P.A. Tirkas, et al., Finite-difference time-domain method for electromagnetic radiation, interference, and interaction with complex structures, IEEE Trans. Electromagn. Compat. 35 (2) (1993) 192–203.

[166] Y. Hao, R. Mittra, FDTD Modeling of Metamaterials: Theory and Applications, Artech house, 2008.

[167] C.A. Remley, Time Domain Modeling of Electromagnetic Radiation with Application to Ultrafast Electronic and Wireless Communications Systems (PhD Thesi), Oregon State Umiversity, Corvallis, Oregon, USA, 1999.

[168] F. Zheng, Z. Chen, J. Zhang, A finite-difference time-domain method without the courant stability conditions, IEEE Microw. Guid. Wave Lett. 9 (11) (1999) 441–443.

[169] L. Talbi, G. Delisle, Finite difference time domain characterization of indoor radio propagation, Prog. Electromagn. Res. 12 (1996) 251–275.

[170] A.P. de Azevedo, A.J.M. Soares, L.C. Fernandes, Measurements and FDTD simulations of electric fields in indoor environment at 150 MHz, in: Proceedings of the 15th SBMO/IEEE MTT-S International Microwave and Optoelectronics Conference IMOC, Rio de Janeiro, Brazil, 2013.

[171] L. Nagy, Indoor propagation modeling for short range devices, in: The Second European Conference on Antennas and Propagation, EuCAP 2007, IET, 2007, pp. 1–6.

[172] U. Virk, K. Haneda, et al., Full-wave characterization of indoor office environment for accurate coverage analysis, in: International Conference on Electromagnetics in Advanced Applications (ICEAA), IEEE, 2013, pp. 1197–1200.

[173] M. Porebska, T. Kayser, W. Wiesbeck, Verification of a hybrid ray-tracing/FDTD model for indoor ultra-wideband channels, in: 2007 European Conference on Wireless Technologies, IEEE, 2007, pp. 169–172.

[174] L. Nagy, Comparison and application of FDTD and ray optical method for indoor wave propagation modeling, in: Proceedings of the Fourth European Conference on Antennas and Propagation, IEEE, 2010, pp. 1–3.

[175] L. Nagy, FDTD and ray optical methods for indoor wave propagation modeling, in: Mikrotalasna Revija, 2010.

[176] M. Thiel, K. Sarabandi, A hybrid method for indoor wave propagation modeling, IEEE Trans. Antennas and Propagation 56 (8) (2008) 2703–2709.

[177] H. Kim, B. Kim, Y. Lee, An accurate indoor propagation analysis for wi-fi antenna embedded in a commercial TV set, in: The 8th European Conference on Antennas and Propagation (EuCAP 2014), IEEE, 2014, pp. 2111–2114.

[178] G. Wolfle, F. Landstorfer, Field strength prediction in indoor environments with neural networks, in: 1997 IEEE 47th Vehicular Technology Conference, Vol. 1, IEEE, 1997, pp. 82–86.

[179] D. Plets, et al., Coverage prediction and optimization algorithms for indoor environments, EURASIP J. Wireless Commun. Networking 2012 (1) (2012) 1–23.

[180] R. Wahl, et al., Dominant path prediction model for urban scenarios, in: 14th IST Mobile and Wireless Communications Summit, Dresden (Germany), 2005.

[181] G. Wölfle, G. Wol, F. Landstorfer, Field strength prediction with dominant paths and neural networks for indoor mobile communication, 1997.

[182] G. Wolfle, F. Landstorfer, Dominant paths for the field strength prediction, in: VTC 98. 48th IEEE Vehicular Technology Conference, Vol. 1, IEEE, 1998, pp. 552–556.

[183] M.B. Khrouf, et al., Indoor prediction of propagation using dominant path: Study and calibration, in: 2005 12th IEEE International Conference on Electronics, Circuits and Systems, IEEE, 2005, pp. 1–4.

[184] M.C.T. Weiland, Discrete electromagnetism with the finite integration technique, Prog. Electromagn. Res. 32 (2001) 65–87.

[185] T. Weiland, A discretization model for the solution of Maxwell's equations for six-component fields, Arch. Elektron. Uebertrag.tech. 31 (1977) 116–120.

[186] M. Studio, CST-computer simulation technology, 2017, [Online]. Available, Accessed on: 10/02/2017.

[187] T. Weiland, Time domain electromagnetic field computation with finite difference methods, Int. J. Numer. Modelling, Electron. Netw. Devices Fields 9 (4) (1996) 295–319.

[188] P. Zakharov, et al., Comparative analysis of ray tracing, finite integration technique and empirical models using ultra-detailed indoor environment model and measurements, in: 2009 3rd IEEE International Symposium on Microwave, Antenna, Propagation and EMC Technologies for Wireless Communications, IEEE, 2009, pp. 169–176.

[189] G.K. Theofilogiannakos, T.D. Xenos, T.V. Yioultsis, A hybrid parabolic equation—Integral equation technique for wave propagation modeling of indoor communications, IEEE Trans. Magn. 45 (3) (2009) 1112–1115.

[190] I. Kavanagh, et al., A method of moments based indoor propagation model, in: 2015 9th European Conference on Antennas and Propagation (EuCAP), IEEE, 2015, pp. 1–5.

[191] Z. Sandor, et al., 3D ray launching and moment method for indoor radio propagation purposes, in: The 8th IEEE International Symposium on Personal, Indoor and Mobile Radio Communications, 1997. Waves of the Year 2000. PIMRC'97, Vol. 1, IEEE, 1997, pp. 130–134.

[192] I.T.U. ITU, Effects of building materials and structures on radiowave propagation above about 100 MHz, in: Recommendation ITU-R P.2040-1, Electronic Publication, ed. Geneva, 2015.

[193] F.T. Ulaby, U. Ravaioli, Fundamentals of Applied Electromagnetics 7e, Prentice Hall, 2015.

[194] S. Stavrou, S. Saunders, Review of constitutive parameters of building materials, in: Twelfth International Conference on Antennas and Propagation, (ICAP 2003). (Conf. Publ. No. 491), Vol. 1, IET, 2003, pp. 211–215.

[195] Y. Abdallah, A. Liu, Characterization of indoor penetration loss at ISM band mohammed, in: Environmental Electromagnetics. CEEM, 2003, pp. 4–7.

[196] A. Safaai-Jazi, S.M. Riad, A. Muqaibel, A. Bayram, Ultra-wideband propagation measurements and channel modeling, in: DARPA NETEX Time Domain and RF Measurement Laboratory, Virginia, 2002.

[197] F. Sagnard, G.E. Zein, In situ characterization of building materials for propagation modeling: Frequency and time responses, IEEE Trans. Antennas and Propagation 53 (10) (2005) 3166–3173.

[198] I. Cuiñas, M.G. Sánchez, Permittivity and conductivity measurements of building materials at 5.8 GHz and 41.5 GHz, Wirel. Pers. Commun. 20 (1) (2002) 93–100.

[199] J. Jemai, T. Kumer, A. Varone, J.-F. Wagen, Determination of the permittivity of building materials through WLAN measurements at 2.4 GHz, in: 2005 IEEE 16th International Symposium on Personal, Indoor and Mobile Radio Communications, Vol. 1, IEEE, 2005, pp. 589–593.
[200] F.A.K. Kakar, K.A. Sani, F. Elahi, Essential factors influencing building penetration loss, in: 11th IEEE International Conference on Communication Technology, ICCT 2008, 2008, pp. 1–4.
[201] G. Durgin, T.S. Rappaport, H. Xu, Measurements and models for radio path loss and penetration loss in and around homes and trees at 5.85 GHz, IEEE Trans. Commun. 46 (11) (1998) 1484–1496.
[202] G. Durgin, T.S. Rappaport, H. Xu, 5.85-GHz radio path loss and penetration loss measurements in and around homes and trees, IEEE Commun. Lett. 2 (3) (1998) 70–72.
[203] G. Durgin, T.S. Rappaport, H. Xu, Radio path loss and penetration loss measurements in and around homes and trees at 5.85 GHz, in: Antennas and Propagation Society International Symposium, 1998. IEEE, Vol. 2, IEEE, 1998, pp. 618–621.
[204] S. Celik, et al., Indoor to outdoor propagation model improvement for gsm900/gsm1800/CDMA-2100, in: 2011 XXXth URSI General Assembly and Scientific Symposium, 2011, pp. 1–4.
[205] S. Aguirre, L.H. Loew, Y. Lo, Radio propagation into buildings at 912, 1920, and 5990 MHz using microcells, in: 1994 Third Annual International Conference on Universal Personal Communications, 1994. Record, IEEE, 1994, pp. 129–134.
[206] P.I. Wells, The attenuation of UHF radio signals by houses, IEEE Trans. Veh. Technol. 26 (4) (1977) 358–362.
[207] L. Ferreira, et al., Characterisation of signal penetration into buildings for GSM and UMTS, in: 3rd International Symposium on Wireless Communication Systems, ISWCS'06, IEEE, 2006, pp. 63–67.
[208] T. Schwengler, M. Glbert, Propagation models at 5.8 GHz-path loss and building penetration, in: RAWCON 2000. 2000 IEEE Radio and Wireless Conference (Cat. No. 00EX404), IEEE, 2000, pp. 119–124.
[209] R. Gahleitner, E. Bonek, Radio wave penetration into urban buildings in small cells and microcells, in: Proceedings of IEEE Vehicular Technology Conference (VTC), IEEE, 1994, pp. 887–891.
[210] J. Medbo, et al., Multi-frequency path loss in an outdoor to indoor macrocellular scenario, in: 3rd European Conference on Antennas and Propagation, 2009. EuCAP 2009, IEEE, 2009, pp. 3601–3605.
[211] T.B. Gibson, D.C. Jenn, Prediction and measurement of wall insertion loss, 1999.
[212] D.M. Rose, T. Kürner, Outdoor-to-indoor propagation—Accurate measuring and modelling of indoor environments at 900 and 1800 MHz, in: 2012 6th European Conference on Antennas and Propagation (EUCAP), IEEE, 2012, pp. 1440–1444.
[213] H. Elgannas, I. Kostanic, Outdoor-to-indoor propagation characteristics of 850 MHz and 1900 MHz bands in macro cellular environments, in: Proceedings of the World Congress on Engineering and Computer Science (WCECS'14), 2014.
[214] I. Rodriguez, et al., Path loss validation for urban micro cell scenarios at 3.5 GHz compared to 1.9 GHz, in: 2013 IEEE Global Communications Conference (GLOBECOM), IEEE, 2013, pp. 3942–3947.
[215] A. De Toledo, A. Turkmani, Propagation into and within buildings at 900, 1800 and 2300 MHz, in: [1992 Proceedings] Vehicular Technology Society 42nd VTS Conference-Frontiers of Technology, IEEE, 1992, pp. 633–636.
[216] A. Davidson, C. Hill, Measurement of building penetration into medium buildings at 900 and 1500 MHz, IEEE Trans. Veh. Technol. 46 (1) (1997) 161–168.
[217] W.J. Tanis, G.J. Pilato, Building penetration characteristics of 880 MHz and 1922 MHz radio waves, in: IEEE 43rd Vehicular Technology Conference, IEEE, 1993, pp. 206–209.
[218] N.J. LaSorte, W.J. Barnes, H.H. Refai, Experimental characterization of building penetration loss of a hospital from 55-1950 MHz, studies 649 (050) (2009) 135.
[219] I. Rodriguez, et al., Radio propagation into modern buildings: Attenuation measurements in the range from 800 MHz to 18 GHz, in: IEEE 80th Vehicular Technology Conference (VTC Fall), IEEE, 2014, pp. 1–5.
[220] H. Okamoto, K. Kitao, S. Ichitsubo, Outdoor-to-indoor propagation loss prediction in 800-MHz to 8-GHz band for an urban area, IEEE Trans. Veh. Technol. 58 (3) (2009) 1059–1067.
[221] B.D. Backer, et al., The study of wave-propagation through a windowed wall at 1.8 GHz, in: Proceedings of Vehicular Technology Conference-VTC, Vol. 1, IEEE, 1996, pp. 165–169.
[222] M. Kvicera, P. Pechac, Building penetration loss for satellite services at L-, S- and C-band: Measurement and modeling, IEEE Trans. Antennas and Propagation 59 (8) (2011) 3013–3021.
[223] M. Kvicera, et al., Building penetration loss measurements for satellite-to-indoor systems: Preliminary results, in: 2010 Proceedings of the Fourth European Conference on Antennas and Propagation (EuCAP), IEEE, 2010, pp. 1–4.
[224] D.I. Axiotis, M.E. Theologou, Building penetration loss at 2 GHz for mobile communications at high elevation angles by HAPS, in: The 5th International Symposium on, Wireless Personal Multimedia Communications, Vol. 1, IEEE, 2002, pp. 282–285.
[225] K.L. Chee, et al., Outdoor-to-indoor propagation loss measurements for broadband wireless access in rural areas, in: Proceedings of the 5th European Conference on Antennas and Propagation (EUCAP), IEEE, 2011, pp. 1376–1380.
[226] Y. Miura, Y. Oda, T. Taga, Outdoor-to-indoor propagation modelling with the identification of path passing through wall openings, in: The 13th IEEE International Symposium on Personal, Indoor and Mobile Radio Communications, Vol. 1, IEEE, 2002, pp. 130–134.
[227] E. Suikkanen, A. Tölli, M. Latva-aho, Characterization of propagation in an outdoor-to-indoor scenario at 780 MHz, in: 21st Annual IEEE International Symposium on Personal, Indoor and Mobile Radio Communications, IEEE, 2010, pp. 70–74.
[228] M. Alatossava, et al., Extension of COST 231 path loss model in outdoor-to-indoor environment to 3.7 Ghz and 5.25 Ghz, in: 11th International Symposium on Wireless Personal Multimedia Communications (WPMC), Vol. 8, 2008, pp. 214–218.
[229] C. Hägerling, C. Ide, C. Wietfeld, Coverage and capacity analysis of wireless M2M technologies for smart distribution grid services, in: 2014 IEEE International Conference on Smart Grid Communications (SmartGridComm), IEEE, 2014, pp. 368–373.
[230] C. Müller, et al., Performance analysis of radio propagation models for smart grid applications, in: 2011 IEEE International Conference on Smart Grid Communications (SmartGridComm), IEEE, 2011, pp. 96–101.
[231] M. Alatossava, et al., Comparison of outdoor to indoor and indoor to outdoor MIMO propagation characteristics at 5.25 GHz, in: 2007 IEEE 65th Vehicular Technology Conference-VTC2007-Spring, IEEE, 2007, pp. 445–449.
[232] S.Y. Lim, Z. Yun, J.M. Baker, N. Celik, H.-s. Youn, M.F. Iskander, Propagation modeling and measurement for a multifloor stairwell, IEEE Antennas Wirel. Propag. Lett. 8 (2009) 583–586.
[233] S.Y. Lim, Z. Yun, M.F. Iskander, Propagation measurement and modeling for indoor stairwells at 2.4 and 5.8 GHz, IEEE Trans. Antennas and Propagation 62 (9) (2014) 4754–4761.